



**UNIVERSITY OF LEEDS**

This is a repository copy of *Suppression of marine ice sheet instability*.

White Rose Research Online URL for this paper:

<http://eprints.whiterose.ac.uk/137914/>

Version: Accepted Version

---

**Article:**

Pegler, SS [orcid.org/0000-0001-8373-2693](https://orcid.org/0000-0001-8373-2693) (2018) Suppression of marine ice sheet instability. *Journal of Fluid Mechanics*, 857. pp. 648-680. ISSN 0022-1120

<https://doi.org/10.1017/jfm.2018.742>

---

© 2018 Cambridge University Press. This article has been published in a revised form in *Journal of Fluid Mechanics* [<https://doi.org/10.1017/jfm.2018.742>]. This version is free to view and download for private research and study only. Not for re-distribution, re-sale or use in derivative works. Uploaded in accordance with the publisher's self-archiving policy.

**Reuse**

Items deposited in White Rose Research Online are protected by copyright, with all rights reserved unless indicated otherwise. They may be downloaded and/or printed for private study, or other acts as permitted by national copyright laws. The publisher or other rights holders may allow further reproduction and re-use of the full text version. This is indicated by the licence information on the White Rose Research Online record for the item.

**Takedown**

If you consider content in White Rose Research Online to be in breach of UK law, please notify us by emailing [eprints@whiterose.ac.uk](mailto:eprints@whiterose.ac.uk) including the URL of the record and the reason for the withdrawal request.



[eprints@whiterose.ac.uk](mailto:eprints@whiterose.ac.uk)  
<https://eprints.whiterose.ac.uk/>

## Suppression of marine ice sheet instability

Journal:	<i>Journal of Fluid Mechanics</i>
Manuscript ID	JFM-17-S-0443.R4
mss type:	JFM Papers
Date Submitted by the Author:	11-Sep-2018
Complete List of Authors:	Pegler, Sam; University of Leeds, School of Mathematics
Keyword:	Ice sheets < Geophysical and Geological Flows, Instability, Channel flow < Waves/Free-surface Flows

SCHOLARONE™  
Manuscripts

# Suppression of marine ice sheet instability

Samuel S. Pegler

School of Mathematics, University of Leeds, Leeds LS2 9JT, UK

(Received 11 September 2018)

A long-standing open question in glaciology concerns the propensity for ice sheets that lie predominantly submerged in the ocean (marine ice sheets) to destabilise under buoyancy. This paper presents a study of the mechanisms by which a buoyancy-driven mechanism for the retreat and ultimate collapse of such ice sheets – the marine ice sheet instability – is suppressed by lateral stresses acting on its floating component (the ice shelf). The key results are to demonstrate the transition between a mode of *stable* (easily reversible) retreat along a stable steady-state branch created by ice-shelf buttressing to *tipped* (almost irreversible) retreat across a critical parametric threshold. The conditions for triggering tipped retreat can be controlled by the calving position and other properties of the ice-shelf profile and weakly dependent on basal stress, in contrast to principles established from studies of unbuttressed grounding-line dynamics. The stability and recovery conditions introduced by lateral stresses are analysed by developing a method of constructing grounding-line stability (bifurcation) diagrams, which provide a rapid assessment of the steady-state positions, their natures and the conditions for secondary grounding, giving clear visualisations of global stabilisation conditions. A further result is to reveal the possibility of a third structural component of a marine ice sheet that lies intermediate to the fully grounded and floating components. The region forms an extended grounding *area* in which the ice sheet lies very close to flotation, and there is no clearly distinguished grounding line. The formation of this region generates an upsurge in buttressing that provides the most feasible mechanism for reversal of a tipped grounding line. The results of this paper provide conceptual insight into the phenomena controlling the stability of the West Antarctic Ice Sheet, the collapse of which has the potential to dominate future contributions to global sea-level rise.

---

## 1. Introduction

The total or partial collapse of the West Antarctic Ice Sheet (WAIS) – the largest example of a so-called marine ice sheet – has the potential to increase global sea level independently by several metres over the course of the next few centuries (Bamber *et al.* 2009; Hanna *et al.* 2013). However, the conditions controlling its destabilisation are currently poorly understood. A marine ice sheet is a continent scale glacial mass that lies submerged in the ocean. Since ice is lighter than water, buoyancy acts to detach a marine ice sheet from the underlying bedrock. This has led to a long-standing open problem in glaciology regarding the conditions under which buoyancy drives a marine ice sheet to collapse, a principle known as the ‘marine sheet instability’ (MISI) (Weertman 1974; Thomas & Bentley 1978). The essential likelihood of instability, the mode and time scales on which it may be triggered, remain key unknowns in efforts to assess contributions to future sea-level rise. A potentially key mechanism for suppressing instability is an effect of the peripheral floating regions of the ice sheet (the ice shelves) in creating a buttress

42 that supports the considerably larger grounded interior of the ice sheet against surg-  
 43 ing outwards into the ocean (Hughes 1981; Stuiver *et al.* 1981). The process of ice-shelf  
 44 buttressing may be key to understanding marine ice sheet collapse, providing a strong  
 45 motivation to explore its mechanical underpinnings. The present paper presents a theo-  
 46 retical investigation of the mechanisms by which the onset of, suppression of and recovery  
 47 from MISI is controlled by lateral stresses and ice-shelf buttressing. A focus is to iden-  
 48 tify parametric tipping points for triggering of a large-scale retreat occurring once the  
 49 conditions for sustaining a stable steady state fail critically.

50 In describing the onset of MISI, I distinguish two different modes of grounding-line  
 51 retreat. Following changing external parametric conditions (e.g. a reduction in snow  
 52 accumulation rate or an increase in the rate of melting of the ice shelf), a grounding  
 53 line may retreat towards a new stable steady state near the present grounding line. In  
 54 this mode of ‘stable’ retreat, the grounding line will recover to its original position if  
 55 parameters are subsequently restored to their former values. If the changing external  
 56 conditions instead lead to a removal of the possibility of a stable steady state near  
 57 the present state, then a more sudden and sustained retreat can instigate from which  
 58 recovery may be impossible following even complete parametric restoration. The onset  
 59 of this mode of ‘tipped’ retreat can be identified with the notion of MISI.

60 The main analytical tool I use is the steady-state balance equation for the grounding-  
 61 line position  $x_G$  (Pegler 2018),

$$E[d(x_G)] + B(x_G, x_C) = \frac{1}{2}\rho g' d(x_G)^2, \quad (1.1)$$

62 where  $d(x)$  is the flotation profile (related to the bed profile),  $E$  is the depth-integrated  
 63 longitudinal extensional stress,  $B$  is the ice-shelf buttressing force,  $x_C$  is the calving posi-  
 64 tion of the ice shelf,  $\rho$  is the density and  $g'$  is the reduced gravity. The functions  $E[d(x_G)]$   
 65 and  $B(x_G, x_C)$  represent universal analytical functions of the grounding-line position  $x_G$   
 66 that are derived from integrations of the grounded and floating components of a quasi-  
 67 two-dimensional (Q2D) model (to be reviewed in §2). The Q2D model is defined as a  
 68 flow-line model (Dupont & Alley 2005; Nick *et al.* 2010; Hindmarsh 2012; Pegler *et al.*  
 69 2013; Walker *et al.* 2013; Pegler 2016; Kowal *et al.* 2016; Schoof *et al.* 2017) with use of a  
 70 parametrisation of the transverse viscous shear stress for hard margins (Pegler 2016). The  
 71 algebraic equation (1.1) determines the steady-state grounding-line positions consider-  
 72 ably faster than numerical analysis based on the full two-dimensional SSA equations (e.g.  
 73 Gudmundsson *et al.* 2012), but nonetheless recovers its steady-state predictions to good  
 74 approximation subject to certain caveats, including the approximation of a reasonably  
 75 parallel flow (see the supplementary document, §2 and §8.3 of Pegler 2018, for a discussion  
 76 of the results of the comparison study and the anticipated limitations of the theory). As  
 77 will be shown via the analysis of tipping conditions in the present paper, the evaluation  
 78 of the current steady states for a given set of parameters, as predicted by the analytical  
 79 functions comprising (1.1), is sufficient to indicate the future state towards which any  
 80 *time-dependent* grounding line can stabilise under a given parametric configuration.

81 Equation (1.1) elucidates the general control of a grounding line across the spectrum  
 82 bridging the unbuttressed (extension-dominated) balance,  $E(d) \sim (\rho g'/2)d^2$  (e.g. Weert-  
 83 man 1974; Muszynski & Birchfield 1987; Chugunov & Wilchinsky 1996; Wilchinsky &  
 84 Chugunov 2000; Schoof 2007a,b; Robison *et al.* 2010; Tsai *et al.* 2015) to a limiting  
 85 regime of strong ice-shelf buttressing,  $B(x_G, x_C) \sim (\rho g'/2)d^2$  arising for strongly con-  
 86 fined marine-terminating glaciers (Pegler *et al.* 2013). The limiting end members of (1.1)  
 87 exhibit markedly different dependences on the properties of a given marine ice sheet. For  
 88 example, the extensional balance is completely independent of calving position  $x_C$  but  
 89 inherently sensitive to basal stress. By contrast, the strongly buttressed balance is inde-

90 pendent of basal stress but centrally dependent on the calving position  $x_C$ . The theory  
 91 underlying (1.1) will break down if the ice shelf associated with the steady state makes  
 92 further contacts with the bedrock downstream of the grounding line, a situation referred  
 93 to as secondary grounding (encompassing either the formation of an ice rise or an imme-  
 94 diate reconnection between the ice shelf and the bedrock in front of the grounding line).  
 95 The inducement of secondary grounding by lateral stresses will be shown in this paper  
 96 to provide a the first mechanism that comes into play in order to reverse tipped retreat.

97 Analysis of horizontally one-dimensional (unbuttressed) marine ice sheets has shown  
 98 that the migration of the grounding line is controlled by the flotation thickness  $d$  (e.g.  
 99 Schoof 2007*b*). This dependence can be recovered by the unbuttressed reduction of the  
 100 grounding-line balance of (1.1) to  $E(d) \sim (\rho g' / 2) d^2$ , which represents an implicit equa-  
 101 tion for  $d$  only. This thickness-dominated control can be reduced to a relationship between  
 102 grounding-line thickness and volumetric flux for steady or quasi-steady flow (Chugunov  
 103 & Wilchinsky 1996; Wilchinsky & Chugunov 2000; Schoof 2007*a,b*). As a consequence of  
 104 this relationship, the retreat of a grounding line on a positive bed slope (sloping upwards  
 105 in the direction of flow, also termed reverse or retrograde) increases the flux across the  
 106 grounding line, producing a positive feedback response. An unbuttressed steady state on  
 107 a positive slope thus provides a local repeller for the evolution of the ice sheet. Con-  
 108 versely, an unbuttressed steady state on a negative bed slope is stable and provides a  
 109 local attractor for the evolution of the ice sheet. Much of the bedrock underlying the  
 110 WAIS deepens towards the centre of Antarctica owing to isostatic depression, creating  
 111 the potential for tipping into positive-feedback retreat.

112 With buttressing included, (1.1) introduces a dependence on the properties of the ice  
 113 shelf, including the calving position  $x_C$ , which precludes the simplified reduction of (1.1)  
 114 to a grounding-line balance dependent purely on the grounding-line thickness  $d$ , which  
 115 applies uniquely in the unbuttressed situation. The associated scaling relationship for ice  
 116 flux then fails to apply, along with the direct relationship between the nature of stability  
 117 and local basal slope. The incorporation of ice-shelf buttressing in flow models has re-  
 118 vealed a number of different stability properties (MacAyeal 1989; Dupont & Alley 2005;  
 119 Goldberg *et al.* 2009; Gagliardini *et al.* 2010; Gudmundsson *et al.* 2012; Gudmundsson  
 120 2013). In particular, it is established that a buttressed grounding line can stabilise on a  
 121 positive bed slope (e.g. Gudmundsson *et al.* 2012). This is possible because grounding-  
 122 line retreat will, at least under the assumption of a fixed calving position, result in an  
 123 increase in the shelf length and hence the buttressing force, potentially counteracting the  
 124 increase in the buoyancy force associated with the retreat. Schoof *et al.* (2017) consider  
 125 the question of establishing local stability for two alternative calving laws: one where  
 126 calving occurs directly at the grounding line, and the other where an ice shelf forms  
 127 and fractures in accordance with a hydrofracture model (Nick *et al.* 2010). In the former  
 128 case, lateral stresses only affect the grounded region (a case not considered here), and  
 129 it is found that the flux can be controlled by a different scaling resulting from lateral  
 130 stresses, as discussed in the context of the calving front of a confined ice shelf (Hind-  
 131 marsh 2012; Pegler 2016). For the hydrofracture model, the calving condition is reduced  
 132 to a condition of a prescribed terminal calving thickness, resulting in a different relation-  
 133 ship between the rate of increase of the buttressing force and the rate of retreat of the  
 134 grounding line as compared to the case of a direct imposition of the calving position. The  
 135 results demonstrate the sensitivity of the establishment of local stability to the choice of  
 136 the calving law, and find that stability is also possible on a retrograde slope under this  
 137 alternative calving model.

138 The present paper will address the questions of how a marine ice sheet transitions  
 139 (tips) into, is suppressed against and recovers from marine ice sheet instability follow-

140 ing continuous parametric variations. The two distinct goals are, first, to construct and  
 141 verify bifurcation diagrams from which the conditions for inducing collapse, maintaining  
 142 stability and recovering following tipping can be inferred. The analysis will elucidate how  
 143 maintenance of the stability of an ice sheet can be assessed on the basis of the critical  
 144 conditions for the instantaneous existence of stable steady states for a given configuration  
 145 of parameters in a time-dependent setting. The second goal is to generate a parameter–  
 146 regime diagram showing the critical conditions separating the situations guaranteeing  
 147 stability, guaranteeing tipping and those for which the question of stabilisation is sub-  
 148 ject to hysteresis. The bifurcation diagrams employ the steady-state database functions  
 149 for steady-state grounding-line forces given by (1.1) in conjunction with conditions for  
 150 secondary grounding (Pegler 2018). The inferred conditions for stabilisation are corrob-  
 151 orated using transient solutions. The analysis of transience identifies in particular a new  
 152 tertiary ice-sheet flow regime – lying in between floating and grounded region – through  
 153 which the flow lies very close to floating over an extended distributed grounding *area*.  
 154 The formation of such a zone is found to provide the most readily available pathway to  
 155 reversal of tipped marine ice sheet instability.

156 I begin in §2 by reviewing the Q2D model and its dimensionless form. This is followed  
 157 in §3 by the development of the primary theoretical tool referred to as the ‘stability  
 158 diagram’, which is a bifurcation diagram in which steady states, their local stability  
 159 and the conditions for secondary grounding are incorporated simultaneously. Section 4  
 160 applies this method to determine the stability of buttressed groundings and elucidates  
 161 new features associated with the ice-sheet structure during the recovery of a tipped  
 162 grounding line. Section 5 considers the general regime diagram describing the conditions  
 163 for tipping and recovery. In §6, corresponding results incorporating power-law rheology  
 164 and transitions to instability based on the retreat of the calving front and the increase  
 165 in melt rate are demonstrated. I end in §7 by summarising the key findings.

## 166 2. Model

167 Consider a marine ice sheet comprising a viscous fluid layer (ice) of density  $\rho$  flow-  
 168 ing over a rigid bed  $z = b(x)$  and lying submerged in an effectively inviscid fluid (the  
 169 ocean) of larger density  $\rho_w$  and upper surface  $z = 0$  (figure 1). The flow is subject to  
 170 a no-slip condition along the margins,  $y = \pm w(x)$ . The flow is modelled using a quasi-  
 171 two-dimensional model that models the two-dimensional viscous stresses associated with  
 172 transverse shearing across the width of the flow, but approximated as retaining an ap-  
 173 proximately one-dimensional thickness profile,  $H(x, t)$ . A corroboration of the accuracy  
 174 of this model is provided in the companion paper (Pegler 2018). The ice sheet generally  
 175 comprises both a grounded region and a floating region – the ice shelf – which interface  
 176 at the grounding line  $x_G(t)$ . The grounded and floating regions can be determined at any  
 177 given time by comparing the thickness profile  $H(x, t)$  to the so-called flotation profile

$$d(x) \equiv -(\rho_w/\rho)b(x), \quad (2.1)$$

178 which represents the threshold thickness below which the ice sheet would float at the  
 179 location  $x$ . If  $H(x, t) > d(x)$ , the flow is grounded at  $x$  and if  $H(x, t) < d(x)$ , it is  
 180 floating.

181 The flow is modelled as an extensional thin-layer flow with differing forms of drag  
 182 and gravitational forces acting on the grounded and floating components. Ice rheology  
 183 is typically modelled as a shear-thinning power-law fluid, with stress proportional to the  
 184 rate of deformation raised to the power  $m = 1/n$ , where  $n$  is typically taken as 3.

Following the companion paper, I model the dynamics using the quasi-two-dimensional

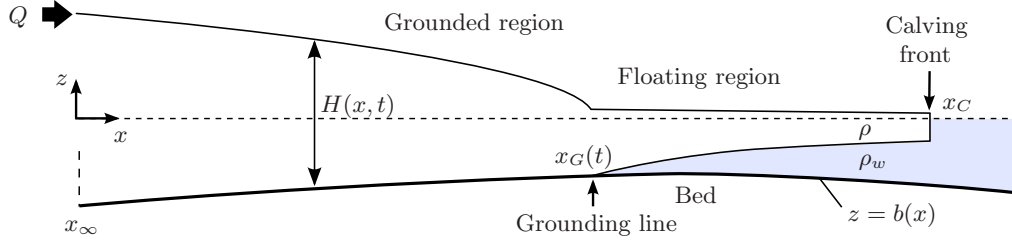


FIGURE 1. Schematic of a marine ice sheet.

(Q2D) model defined by the conditional extensional-flow equation

$$4 \frac{\partial}{\partial x} \left( \mu w H \frac{\partial u}{\partial x} \right) = \begin{cases} D(u) + \rho g w H \left( \frac{\partial H}{\partial x} + \frac{db}{dx} \right) & \text{if } H > d(x), \\ C_+(x) H u^{m_+} + \rho g' w H \frac{\partial H}{\partial x} & \text{if } H < d(x), \end{cases} \quad (2.2a,b)$$

185 where  $u(x, t)$  is the width-averaged velocity,  $\mu = \mu_0 |\partial u / \partial x|^{m_- - 1}$  is the effective viscosity,  
 186  $\mu_0$  is the coefficient of viscosity,  $w(x)$  is the half width of the embayment (assumed  
 187 uniform in the later examples of this paper),  $C_+(x)$  is the effective lateral drag coefficient,  
 188  $g$  is the gravitational strength, and  $g' \equiv (\rho_w - \rho)g / \rho_w$  is the reduced gravity. I model the  
 189 total drag as the sum of the width-integrated basal and depth-integrated lateral stresses,

$$D(u) = w \tau_b(u) + H \tau_s(u) = C_-(x) w u^{m_-} + C_+(x) H u^{m_+}, \quad (2.3)$$

190 where  $C_-(x)$  is the basal drag coefficient and  $m_-$  is the basal drag-law exponent. The  
 191 basal stress is modelled here using a Weertman slip condition (a power-law Navier condi-  
 192 tion), which is standard in ice-sheet simulation (Cuffey & Paterson 2010). The lat-  
 193 eral stress is instead formulated in (2.3) on the basis of a ‘shear-drag parametrisation’,  
 194 which models the lateral stress heuristically as the drag stress associated with a shear-  
 195 dominated transverse shear profile. For this model to be consistent with both the regime  
 196 of transverse-shear-dominated flow and conservation of mass, the effective lateral drag  
 197 coefficient must be taken as  $C_+(x) = \mu_0 [2^{1-n} (n+2)^{-1} w(x)]^{-(1/n)}$  with  $m_- = m$  (Pegler  
 198 2016). This heuristic parametrisation of lateral shear drag yields model predictions that  
 199 are, subject to the approximation of a suitably parallel flow, in good agreement with labo-  
 200 ratory data and two-dimensional simulation of the full SSA equations across the range  
 201 of wide to narrow geometries (Pegler 2016, 2018).

202 It should be noted that the direct summation of the two drag laws used to describe  
 203 the total stress in the grounded region (2.3) is, while likely a good approximation, not  
 204 necessarily accurate unless either basal or lateral stress is locally dominant. For situations  
 205 where the width-integrated basal and depth-integrated lateral stresses are comparable  
 206 in the grounded region, a resolution of a Poiseuille-type transverse elliptic boundary-  
 207 value problem could be conducted to describe a total drag on the grounded region  $D(u)$   
 208 resulting from the mixture of basal and lateral stresses. Nonetheless, it can be anticipated  
 209 that the simple addition of the two drag laws used in (2.3) may, in addition to its clear  
 210 validity in the limits of either one of the contributions being much greater than the other,  
 211 provide a good general approximation for  $D(u)$ , but will be tested with further work.

212 It is worth emphasising that lateral stresses in the ice shelf and lateral stresses in the  
 213 grounded region generally can have very different roles in large-scale ice-sheet dynamics.  
 214 The role of all drag stresses in the grounded region (lateral or basal) is to control the  
 215 steepness of the ice sheet upstream of the grounding line, and hence the amount of



216 ‘pile-up’ for a given grounding-line position. As discussed in Pegler (2018), these stresses  
 217 do not necessarily have an important control of the grounding line, which is controlled  
 218 instead specifically by the resistance to flow across it. The drag stresses a short distance  
 219 upstream of the grounding line play some role in influencing the extensional contribution  
 220 to the resistance to flow across the grounding line, as represented by  $E$  in (1.1). For  
 221 sufficiently large buttressing  $B$ , this contribution can, however, become small even for a  
 222 relatively short ice shelf and the control of the flux and position of the grounding line  
 223 switches to being controlled by the ice shelf (Pegler 2018). The lateral stresses exerted  
 224 in the floating region contributes directly to the resistance to flow across the grounding  
 225 line and hence its position and, in turn, the stability of the entire ice sheet.

226 The considerably greater significance of lateral stresses in the floating region compared  
 227 to lateral stresses in the grounded region can thus be understood by considering the  
 228 forces against which they compete for significance. For flow in the grounded region, the  
 229 competing stress is basal stress. For the flow across the grounding line, the competing  
 230 stress is the extensional stress  $E$ . Since the magnitude of the extensional stress would, in  
 231 the absence of ice-shelf buttressing, provide an independent, and potentially very weak,  
 232 resistance to the flow across the grounding line, it is readily possible for the lateral stresses  
 233 in the floating region – despite their small magnitude compared to the basal stresses in  
 234 the grounded region – to provide the dominant resistance to flow across the grounding  
 235 line. In a sense, the resistance to flow across the grounding line in a marine ice sheet  
 236 provides an independent ‘weak link’ in the maintenance of the large-scale ice-sheet mass  
 237 balance, for which the ice-shelf buttressing provides a direct control. Consequently, ice-  
 238 shelf buttressing can have a major independent control of the amount of ice that can be  
 239 stored stably in the grounded region of a marine ice sheet even if generated by a relatively  
 240 small ice shelf and being small in absolute magnitude compared to the accumulated basal  
 241 stresses exerted further upstream.

The symmetry conditions at the ice divide  $x_D$  and the stress condition at the terminus  
 $x_C$  are given by

$$u = 0 \quad \text{at } x = x_D, \quad (2.4)$$

$$\mu \frac{\partial u}{\partial x} = 0 \quad \text{at } x = x_D, \quad (2.5)$$

$$\mu \frac{\partial u}{\partial x} = \frac{\rho g'}{8} H \quad \text{at } x = x_C, \quad (2.6)$$

242 While I treat  $x_C$  as an imposed parameter in the examples of this paper, a more complex  
 243 calving condition, e.g. on the calving thickness (Schoof *et al.* 2017) could be incorporated  
 244 into the analytical toolkit developed in this paper using an extra condition of the implicit  
 245 form  $H(x_C) = H_C$ , where  $H_C$  is a parameter.

246 Finally, the evolution equation for the thickness is

$$\frac{\partial H}{\partial t} = -\frac{1}{w} \frac{\partial}{\partial x} (wHu) + f(x, t), \quad (2.7)$$

247 where  $f(x, t)$  is the net accumulation of ice.

### 248 2.1. Integrated steady-state balance equation

249 It will be demonstrated in this paper that the sustainment of ice-sheet stability can  
 250 be understood by constructing the steady-state solutions for a given configuration of  
 251 parameters. The steady states can be determined by a reduced, integrated theory (Pegler  
 252 2016, 2018), which will be reviewed as follows. In steady state, the mass conservation



253 equation (2.7) can be integrated subject to (2.4) to yield the flux along the flow,

$$q(x) = Hu = \frac{1}{w(x)} \int_{x_D}^x w(\hat{x})f(\hat{x}) d\hat{x}. \quad (2.8)$$

254 On applying this expression along with certain approximations of the components of the  
 255 grounded and floating sections, separate analytical expressions for forces exerted by the  
 256 steady-state profiles of the grounded and floating regions can be derived. By utilising  
 257 these analytical results together, it was determined that the grounding line  $x_G$  satisfies  
 258 the algebraic equation

$$E(x_G) + B(x_G) = \frac{1}{2}\rho g' d(x_G)^2, \quad (2.9)$$

259 where the two functions on the left-hand side can be interpreted as databases that give  
 260 the steady-state extensional stress and the steady-state buttressing force exerted by an  
 261 ice shelf explicitly in terms of the physical parameters and grounding-line position  $x_G$ .  
 262 By integrating the reduced systems representing grounded and floating regions, these  
 263 functions, given here in a general dimensional form, were determined as follows. The  
 264 extensional resistance function is

$$E(x_G) = 4\mu_0 d(x_G) \left[ \frac{u(x_G)}{d(x_G)} \left( \frac{db(x_G)}{dx} + \frac{D[u(x_G)]}{\rho g w(x_G) d(x_G)} \right) \right]^{1/n}, \quad (2.10)$$

265 where  $u(x_G) = q(x_G)/d(x_G)$ . The buttressing resistance function is

$$B(x_G) = \frac{\rho g'}{2} \left[ \left( H_C^N + \frac{N}{\rho g'} \int_{x_G}^{x_C} \frac{C_+(\hat{x})q(\hat{x})^{1/n}}{w(\hat{x})} d\hat{x} \right)^{2/N} - H_C^2 \right], \quad (2.11)$$

266 where  $N = (n + 1)/n$ , and

$$H_C \equiv H(x_C) = \kappa \left[ \left( \frac{\mu_0}{\rho g'} \right)^{n(n+1)} \left( \frac{C_+(x_C)}{\mu_0 w(x_C)} \right)^n q(x_C)^{n+1} \right]^{N^2}. \quad (2.12)$$

267 The constant  $\kappa = 3.28$  for  $n = 3$  (and  $\kappa \approx 8^{1/N^2}$  more generally).

268 The result of (2.9), with (2.10) and (2.11), forms a closed algebraic equation for steady-  
 269 state grounding line positions  $x_G$ , which can be solved at very minimal numerical cost.  
 270 The relative saving in numerical cost compared to full numerical simulation of the SSA  
 271 equations (e.g. Gudmundsson *et al.* 2012) is at least ten orders of magnitude, but the  
 272 numerical precision is similar for suitable geometries. The method thus provides new  
 273 avenues for rapid scenario exploration and sensitivity analysis, in addition to providing  
 274 physical insight into the underlying dynamics. Moreover, it does not suffer issues of spatial  
 275 numerical resolution, which can be a limitation for confident grounding-line prediction.  
 276 In applying these results, a number of caveats should be noted, which are summarised in  
 277 §8.3 of Pegler (2018). This include the assumption of a suitably parallel ice sheet flow,  
 278 which, while typical of many outlets, will be limited in applicability to the context of  
 279 narrow outlets feeding broad ice shelves, for example.

280 In addition to providing a useful counterpart to numerical simulation, the results of  
 281 (2.9)–(2.11) provide physical insight into the parametric control of marine ice sheets.  
 282 The right-hand side of (2.9) represents the driving hydrostatic pressure drop  $(\delta/2)d(x)^2$ ,  
 283 a force which is purely dependent on the grounding-line thickness. The left-hand side  
 284 is the sum of two distinct forces resisting this driving force: the extensional resistance,  
 285  $E$ , and the ice-shelf buttressing force  $B$ , which varies with respect to the calving and  
 286 grounding-line positions,  $x_C$  and  $x_G$ . The equation (3.1) clarifies the bridge between two  
 287 fundamental limiting balances. One is the unbuttressed, extension-dominated balance,

288  $E(x_G) \sim (\delta/2)d(x_G)^2$  (this result will, subject to some further approximation, recover  
 289 the unbuttressed expression for  $Q$  given by Schoof 2007b). In the opposite limit is the  
 290 buttressing-dominated balance,  $B(x_G) \sim (\delta/2)d(x_G)^2$ , which represents a distinct regime  
 291 of grounding-line control referred to as ‘strong buttressing’ and arises in sufficiently  
 292 narrow geometries (Pegler *et al.* 2013). In this regime, the grounding-line dynamics do  
 293 not depend on the basal conditions of the ice sheet (nor indeed any of the contributions  
 294 to the mixed total drag in the grounded region (2.3)).

## 2.2. Example configurations and dimensionless model

296 While the full framework specified above is more general, for the main illustrative so-  
 297 lutions used in this paper I will make a number of specifications designed to distil the  
 298 examples to focusing specifically on the implications of lateral stresses. First, I neglect  
 299 the  $db/dx(x_G)$  in (2.10), which I anticipate to be a good approximation for dimensional  
 300 slopes of order  $10^{-3}$  or less. I will also assume that the coefficient of basal drag  $C_-$ , flow  
 301 width  $w$  and effective lateral drag coefficient  $C_+$ , are uniformly constant along the flow.  
 302 The basal-drag and rheological exponents will be set as equal,  $m_- = m$ , and I will focus  
 303 on the examples of  $n = 1$  and 3.

304 For my illustrative examples, I will also focus on the case of a broad linear slope defined  
 305 by

$$b(x) = b_0 + ax, \quad (2.13)$$

306 where  $|b_0|$  is the depth of the ocean at the reference position  $x = 0$ , and  $a$  is the bed  
 307 slope. Positive slopes,  $a > 0$ , correspond to a bed height that increases in the direction  
 308 of flow (also termed a reverse, or retrograde slope), as is characteristic of many regions  
 309 of the bedrock underlying the West Antarctic Ice Sheet at large scales. Examples of  
 310 nonlinear bed slopes involving a global maximum or global minimum are provided in the  
 311 supplementary document.

312 The input will be specified as being localised at the ice divide

$$f(x) = 2Q\delta(x - x_D), \quad (2.14)$$

313 where  $Q$  is the input flux into the region  $x > x_D$ . It should be noted that the effects of a  
 314 distributed net accumulation and/or loss via melting [negative  $f(x)$ ] is typical across the  
 315 extent of an ice sheet. The case (2.14) nonetheless provides a useful control condition for  
 316 distilling the examples to considering the effects of lateral stresses independently without  
 317 the extra effect of a variable steady-state flux  $q(x)$ . An example of a large-scale distributed  
 318 accumulation  $f(x) \neq 0$  spanning ice divide to terminus is provided by example 4 of the  
 319 supplementary document. The effect of distributed melting along the underside of the ice  
 320 shelf will be considered in §6 in order to demonstrate the manner in which it can trigger  
 321 tipping of a grounding line.

322 I non-dimensionalise (2.2)–(2.7) by defining

$$x \equiv \mathcal{L}\tilde{x}, \quad t \equiv (\mathcal{L}/\mathcal{U})\tilde{t}, \quad (H, b, d) \equiv \mathcal{H}(\tilde{H}, \tilde{b}, \tilde{d}), \quad u \equiv (Q/\mathcal{H})\tilde{u}. \quad (2.15)$$

where

$$\mathcal{H} \equiv \left[ \mu_0 C_-^m \left( \frac{Q^m}{\rho g} \right)^{m+1} \right]^{\frac{1}{k_m}}, \quad \mathcal{L} \equiv \left[ \frac{\mu_0^{m+2} Q^m}{\rho g C_-^{m+1}} \right]^{\frac{1}{k_m}}, \quad (2.16a,b)$$

and  $k_m \equiv (m+1)(m+2) - 1$ . On dropping tildes, the governing equation (2.2) becomes

$$4 \frac{\partial}{\partial x} \left( \mu H \frac{\partial u}{\partial x} \right) = \begin{cases} (1 + SH)u^m + H \left( \frac{\partial H}{\partial x} + \frac{db}{dx} \right) & \text{if } H > d(x), \\ SHu^m + \delta H \frac{\partial H}{\partial x} & \text{if } H < d(x), \end{cases} \quad (2.17a,b)$$

where  $\mu = |\partial u / \partial x|^{m-1}$ . The dimensionless input condition associated with (2.14), the regularity condition (2.5) and the frontal stress condition (2.6) become

$$Hu = 1 \quad \text{at } x = x_{D+}, \quad (2.18)$$

$$\mu \frac{\partial u}{\partial x} = 0 \quad \text{at } x = x_D, \quad (2.19)$$

$$\mu \frac{\partial u}{\partial x} = \frac{\delta}{8} H \quad \text{at } x = x_C. \quad (2.20)$$

where the plus subscript is used to define a limit from the positive  $x$  direction. The evolution equations (2.2a, b) become

$$\frac{\partial H}{\partial t} = -\frac{\partial}{\partial x}(Hu), \quad \dot{x}_C = u(x_C, t). \quad (2.21a,b)$$

In addition to the positions  $x_\infty$  and  $x_C$ , the dimensionless model depends on two dimensionless parameters:

$$S \equiv \frac{\mathcal{H}C_+}{wC_-}, \quad \delta \equiv \frac{g'}{g}, \quad (2.22a,b,c)$$

representing the dimensionless lateral shear-drag coefficient and the density difference, respectively. As estimated in Pegler (2018),  $S = 0-10^{-2}$ , with  $S = 0$  recovering the case of a one-dimensional marine ice sheet. The value  $\delta = 0.1$  will be assumed throughout my analysis. The value  $x_D = -3 \times 10^3$  will be used for my illustrative time-dependent numerical solutions. Finally, the dimensionless form of the linear bed height (2.13) is

$$b(x) = -\beta + \alpha x, \quad \text{where } \alpha \equiv (\mathcal{L}/\mathcal{H})a, \quad \beta \equiv |b_0|/\mathcal{H}, \quad (2.23)$$

323 are a scaled bed slope and reference ocean depth, respectively.

### 324 **3. Construction of a grounding-line stability diagram**

325 This section develops the analytical methodology used to visualise the determinants  
326 of stability of a marine ice sheet for a given configuration. A method is developed based  
327 on the construction of effective stability (bifurcation) diagrams for grounding lines that  
328 unify steady states, the natures of their local stability (attractor versus repeller) and the  
329 inducement of secondary grounding within a single parameter–stability diagram.

#### 330 **3.1. Steady states**

331 The first component of the methodology is provided by the steady-state equation (2.9a).  
332 In dimensionless form, along with the simplifications described in §2.2, this equation  
333 reads

$$E[d(x_G)] + B(x_G, x_C) = \frac{1}{2} \delta d(x_G)^2. \quad (3.1)$$

For linear rheology,  $n = 1$ , the reduced forms of the resistance functions (2.9b, c) are given by

$$E[d(x_G)] \approx 4d(x_G)^{-3}, \quad B(x_G, x_C) = -S(x_C - x_G). \quad (3.2a,b)$$

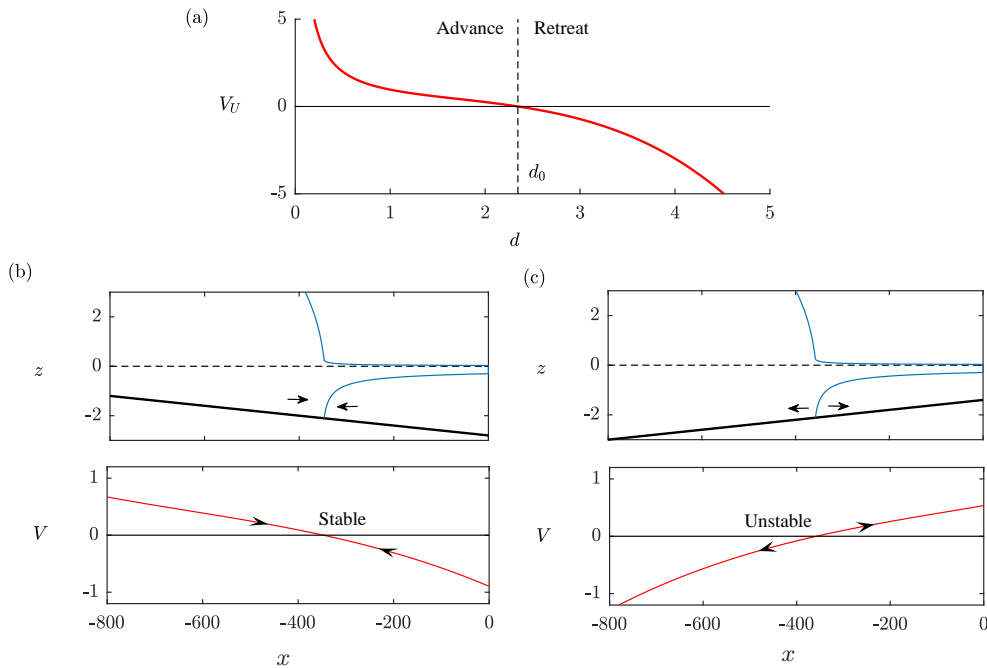


FIGURE 2. The relationship between the stability variable  $V(x) = V_U[d(x)]$  and the grounding-line thickness  $d$  for an unbuttressed grounding line (3.4). In this simplified situation, retreat occurs if the grounding-line thickness  $d$  is larger than the critical value  $d_0$ , and advance occurs if it is less than  $d_0$ , where  $d_0 \approx 2.345$  is the universal dimensionless thickness at which any unbuttressed steady-state grounding line occurs,  $V_U(d_0) = 0$ . Panels (b) and (c) show the stability variable  $V(x)$  predicted by (3.3) for cases of (a) a negative bed slope  $\alpha = -2 \times 10^{-3}$  and  $\beta = 2.8$ , and (b) the positive bed slope  $\alpha = 2 \times 10^{-3}$  and  $\beta = 1.4$ , each with zero buttressing, illustrating stability and instability, respectively. The arrows in the insets show the direction of grounding-line migration following perturbation from the steady state, as implied by the sign of  $V(x)$ .

334 For simplicity, I have here also neglected a contribution to  $E$  owing to the lateral stresses  
 335 in the *grounded* region, represented by the first term in (2.3). These stresses, if comparable  
 336 to the effect of the width-integrated basal stress have a role in controlling the magnitude  
 337 of the thickness gradient upstream of the grounding line and, for sufficiently weak ice-  
 338 shelf buttressing, may have some effect on the grounding line. By contrast, the lateral  
 339 stresses in the floating region are, despite their similar absolute magnitude to the lateral  
 340 stresses in the grounded region, fundamentally more important to ice-sheet stability via  
 341 their leading-order control of the grounding line (Pegler 2018).

342

### 3.2. Local stability

343 A steady-state grounding line position, as predicted by (3.1) and (3.2), will either be an  
 344 attractor (stable) or a repeller (unstable). In the context of unbuttressed grounding-line  
 345 dynamics, a negatively sloped bedrock,  $b'(x_G) < 0$ , generally results in an attractor while  
 346 a positively sloped bedrock results in a repeller (at least subject to the simplification of  
 347 a uniform drag coefficient which, as highlighted at the end of this subsection, can affect  
 348 stability along with any other spatial parametric variation that determines  $E(x)$ ).  
 349 These basic stability results arise because an unbuttressed grounding line perturbed

350 backwards from a steady state on a positive bed slope will increase the grounding-line  
 351 thickness and hence the driving buoyancy force, thereby stimulating further retreat, i.e.  
 352 a positive-feedback response to the original perturbation. Conversely, perturbation of an  
 353 unbuttressed grounding line on a negative slope produces negative feedback and attrac-  
 354 tion back to the original steady state. This has been argued previously on the basis of  
 355 the relationship between grounding-line flux and thickness applicable to an unbuttressed  
 356 grounding line and linear stability analyses (Schoof 2007a; Wilchinsky 2009; Fowler 2011;  
 357 Schoof 2012). These conclusions do not apply to the buttressed case.

358 In order to assess the stability of a general grounding line, I propose a method based  
 359 on evaluating the function

$$V(x) = E[d(x)] + B(x, x_G) - \frac{1}{2}\delta d(x)^2, \quad (3.3)$$

360 which represents the ‘imbalance’ associated with the steady-state forces in (3.1). If  
 361  $V(x_G) = 0$ , there is a steady state at  $x_G$ . The gradient  $V'(x_G)$  will then indicate the  
 362 nature of stability of the steady state at  $x_G$  in the manner of an autonomous evolu-  
 363 tion rule, ‘ $\dot{x} \propto V(x_G)$ ’. To explain this, note first that the function  $V(x_G)$  will indicate  
 364 stability correctly in this way for the unbuttressed case, as I verify directly below. Its  
 365 general functioning is then clear from the fact that the nature of an isolated steady-state  
 366 branch across a bifurcation diagram is conserved under continuous parametric variation.  
 367 A more rigorous proof of the functioning of  $V$  is beyond the scope of this paper but,  
 368 to gain confidence in its functioning, I include a supplementary document with a suite  
 369 of examples validated using time-dependent integrations, in addition to those provided  
 370 later in the paper (figures 5 and 9).

371 Because (3.3) depends purely on known analytic expressions, it affords a versatile di-  
 372 rect assessment of steady states and their local stability that, as far as the qualitative  
 373 question of local stability is concerned, bypasses the need for any linear stability anal-  
 374 ysis or consideration of a flux relationship. The method applies for generalised physical  
 375 situations described by the functions of (2.9) (with or without buttressing). Since any  
 376 determinant of the spatial variation of  $E$  and  $B$  will change  $V$ , it follows that the spatial  
 377 variation in  $x$  of any one of the physical parameters, including rheological variation,  $\mu(x)$ ,  
 378 the net accumulation/melt distributions of the ice sheet and ice shelf,  $f(x)$ , calving laws  
 379 (cf. Schoof *et al.* 2017), spatial variations in the coefficients of basal and lateral drag,  
 380  $C_+(x)$  and  $C_-(x)$ , the flow width  $w(x)$ , and the local slope  $b'(x)$ , will all affect local  
 381 stability. It is worth remarking that, as highlighted at the beginning of this subsection,  
 382 spatial variation in the coefficient of basal drag or indeed any of the other parameters  
 383 controlling  $E$  as defined by (2.10) could, in principle, allow for stability of a grounding  
 384 line on a retrograde slope even in the unbuttressed case. An unbuttressed grounding  
 385 line can therefore form stably on a retrograde slope for suitable spatial variations of the  
 386 determinants of  $E$ .

387 In order to verify that  $V'$  correctly indicates the nature of stability for the simplest  
 388 example of the unbuttressed case,  $B = 0$ , note that, in this case, (3.3) simplifies to

$$V(x) = E[d(x)] - \frac{1}{2}\delta d(x)^2 \equiv V_U[d(x)]. \quad (3.4)$$

389 Uniquely in the unbuttressed case,  $V$  is thus a pure function of the flotation thickness  
 390  $d(x)$ . The plot of  $V_U(d)$ , given in figure 2(a) for  $n = 1$ , shows that a steady state occurs  
 391 wherever the grounding-line thickness equals  $d = d_0 \approx 2.345$ . The plot illustrates that  
 392  $V'_U(d) < 0$ . Thus, on combining this result with the chain rule  $V'(x) = d'(x)V'_U(d)$ ,  
 393 it follows that  $\text{sgn}[V'(x)] = \text{sgn}[b'(x)]$ , confirming that the steady state is stable if  
 394  $b'(x_G) < 0$  and unstable if  $b'(x_G) > 0$ . The value of  $V(x)$  evaluated for examples of a  
 395 negative and a positive bed slope are shown in figures 2(b, c), confirming a stable and

396 unstable state, respectively, in agreement with the time-dependent results of panels (a)  
397 and (c) of figure 3 in Pegler (2018).

398 In addition to providing a clear visualisation of the direction of migration of a perturbed  
399 grounding line, the function  $V(x)$  given by (3.3) provides physical insight into the general  
400 control of stability. If a term comprising  $V$  decreases with  $x$  then the effect it represents  
401 contributes towards stabilisation, and vice versa. For example, buoyancy,  $-(\delta/2)d(x)^2$ ,  
402 creates a stabilising, negative-feedback effect if  $b' < 0$  and a positive-feedback effect if  
403  $b' > 0$ . The extensional resistance  $E[d(x)] = 4d^{-3}$  given by (3.2a) is, like buoyancy, also  
404 a decreasing function of  $d$  and will therefore have a qualitatively similar effect on pro-  
405 moting negative versus positive feedback as the buoyancy force. However, it should be  
406 noted that for  $n = 3$ ,  $E[d(x)] = 4d(x)^{-0.25}$  is only very weakly dependent on  $x$  and thus  
407 has practically no effect on the control of local stability. The buttressing force  $B(x_G, x_C)$ ,  
408 given by (2.9c) or (3.2b), is, in contrast to the functions representing the buoyancy force  
409 and extensional stress, always a decreasing function of the grounding-line position  $x_G$  (a  
410 longer ice shelf generates more buttressing), and thus has an unconditionally stabilising  
411 effect (this is true at least for the case of a prescribed  $x_C$  assumed here; this relationship  
412 is not necessarily as straightforward for cases where  $x_C$  is controlled implicitly by a condi-  
413 tion based on a critical thickness,  $H = H_C$  (Schoof *et al.* 2017)). If  $b'(x) < 0$ , buttressing  
414 will reinforce the stabilising effect of buoyancy on a negative slope. For a positive slope,  
415  $b'(x_G) > 0$ , buttressing and buoyancy act in opposition: retreat of the grounding line will  
416 increase both buoyancy and buttressing. Thus, if the increase in buttressing following a  
417 retreat of a grounding line exceeds the increase in buoyancy critically, then the positive  
418 feedback response, which would occur in the absence of buttressing, will be suppressed.

### 419 3.3. Secondary grounding

The final step of constructing the stability diagram is to determine the grounding-line  
positions  $x$  for which the steady-state profile of the ice shelf produced would experience  
secondary grounding. As described in §6 of Pegler (2018), there are two kinds of secondary  
grounding. Either the ice shelf is predicted to penetrate the bedrock immediately at the  
grounding line (type I) or further downstream (type II). The critical boundary of the  
region of a parameter space in which secondary grounding occurs is given by the critical  
satisfaction of the cotangency conditions between the ice shelf and the bedrock at the  
grounding line,

$$H(x_G) = d(x_G), \quad H'(x_G) = d'(x_G). \quad (3.5a,b)$$

420 This condition represents both the critical transition between no secondary grounding  
421 and type I, as well as the transition between type I and type II. My numerical ap-  
422 proach for determining these transitions is detailed in Pegler (2018), along with the more  
423 straightforward analytical approach available for  $n = 1$ .

424 For grounding-line positions invalidated by secondary grounding, the stability variable  
425 (3.3) fails to apply because the expression for the buttressing force (3.2b) is based on an  
426 assumption of continuous flotation between the grounding line and the calving front. It  
427 will be demonstrated later that the critical occurrence of secondary grounding leads to  
428 a surprising effect of unconditionally reversing tipped grounding-line retreat, with the  
429 direction of grounding-line migration indicated by (3.3) being directly overridden.

## 430 4. The critical transitions into and from marine ice sheet instability

431 Lateral stresses impact ice-sheet stability in three fundamentally distinct ways. One  
432 is to introduce the buttressing force  $B(x_G, x_C)$  directly into the balance equation (3.3).

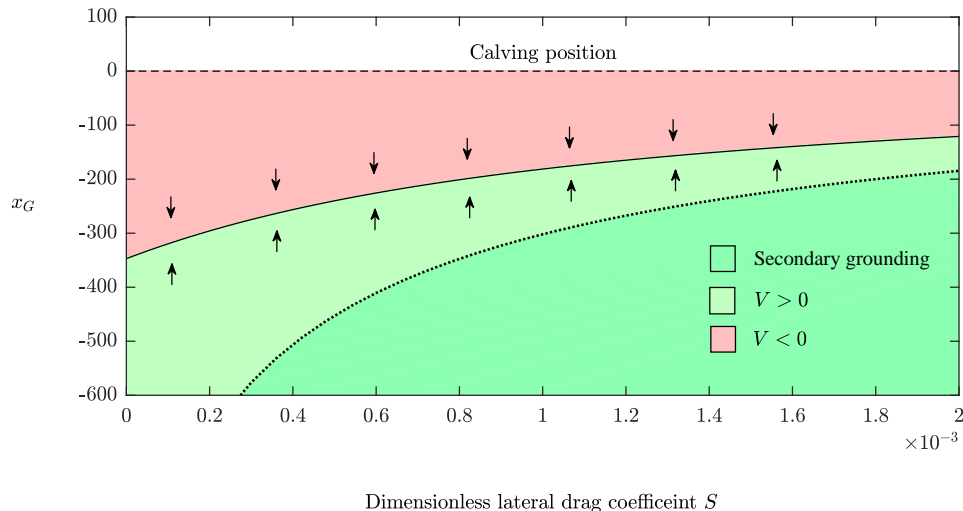


FIGURE 3. The stability diagram for the negative slope  $\alpha = -2 \times 10^{-3}$ , reference ocean depth  $\beta = 2.8$  and calving position  $x_C = 0$ , shown as a continuous variation of the dimensionless lateral shear drag coefficient  $S$ , illustrating its variation from the unbuttressed case  $S = 0$  to buttressed cases  $S > 0$ . The colour scale indicates the sign of the stability variable  $V(x)$  evaluated using (3.3). Green represents grounding-line advancement ( $V > 0$ ) and red represents retreat ( $V < 0$ ). The solution to the steady-state equation (3.1) is shown as a solid curve. The dark green region with a dotted outline represents grounding-line positions for which the steady-state ice shelf produces secondary grounding. The portrait illustrates the existence of a stable steady state for all values of  $S$ .

433 The second is to induce secondary grounding by thickening the ice shelf. A third is the  
 434 contribution to the total drag in the grounded region (2.3). This section will focus on  
 435 demonstrating the first two of these effects and to demonstrate their potential to provide  
 436 the leading-order control of the onset and reversal of tipped grounding-line retreat (ma-  
 437 rine ice sheet instability). The analysis is divided into three subsections – one addressing  
 438 a negative bed slope, and two addressing a positive slope – which account for all the  
 439 qualitatively different regimes of stabilisation that are possible for a broad line slope.

#### 440 4.1. A negative bed slope

441 For a negative bed slope,  $\alpha < 0$ , buoyancy has a stabilising effect, which is reinforced  
 442 by ice-shelf buttressing. To illustrate this explicitly, I construct the stability diagram for  
 443 the example of  $\alpha = -2 \times 10^{-3}$ ,  $\beta = 2.8$  and  $x_C = 0$ , as a continuous variation against  
 444 the drag parameter  $S$ , showing its variation from the unbuttressed case  $S = 0$  to the  
 445 buttressed cases  $S > 0$ . The result is shown in figure 3, where the colour indicates the  
 446 sign of the stability variable  $V(x)$  evaluated using (3.3): red represents retreat ( $V < 0$ ),  
 447 green represents advance ( $V > 0$ ). The steady-state solution to (3.1) is shown as a solid  
 448 curve. The region of the space for which the steady-state ice shelf produces secondary  
 449 grounding is shown coloured darker with a dashed outline. The plot confirms that a  
 450 stable steady state arises for all values of  $S$ . The exclusive effect of lateral stresses is to  
 451 cause the steady state to lie further downstream.

452 It should be noted that the region in which secondary grounding is predicted only  
 453 overlays the region in which  $V > 0$ . Since secondary grounding can only increase the



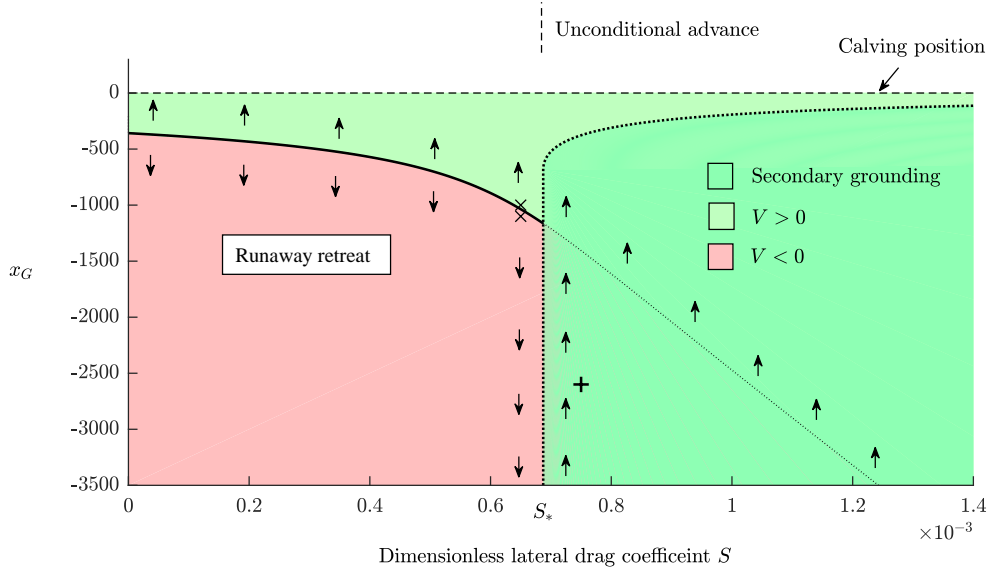


FIGURE 4. The stability diagram for the positive bed slope  $\alpha = 2 \times 10^{-3}$ , reference ocean depth  $\beta = 1.4$  and calving position  $x_C = 0$ , shown as a continuous variation of  $S$ . The colour scale indicates the sign of the stability variable  $V(x)$  evaluated using (3.3). Green represents grounding-line advancement ( $V > 0$ ) and red represents retreat ( $V < 0$ ). The dark green region with a dotted outline represents the region in which secondary grounding is predicted to occur in steady state. As confirmed by the numerical result of figure 5(b), the instance of secondary grounding overrides the direction of stability indicated by (3.3), with the result of producing unconditional grounding-line advance. The solution to (3.1) is shown as a solid curve, and as a dotted curve in the region of secondary grounding. For values of  $S < S_*(\alpha, \beta) \approx 6.9 \times 10^{-4}$ , there is a single unstable steady state. Above the critical value,  $S > S_*(\alpha, \beta)$ , secondary grounding invalidates the steady state and completely suppresses the possibility of runaway retreat, in correspondence with the numerical results of figure 5(b) below. The initial grounding-line positions for the solutions of figure 5(a) are shown as crosses. That of figure 5(b) is shown as a plus sign.

454 buttressing force at the primary grounding line, any secondary grounding will simply  
 455 reinforce the prediction of the stability variable (3.3) that the grounding line advances.  
 456 Therefore, the dark-green region can, in this case, assuredly produce grounding-line ad-  
 457 vancement; a grounding line initiated in the dark green region will advance into the  
 458 lighter green region and on to the steady state.

#### 459 4.2. A positive bed slope

460 For a positive bed slope,  $\alpha > 0$ , the stabilising effect of ice-shelf buttressing instead  
 461 competes against buoyancy, creating richer dynamics. Recall from above that any un-  
 462 buttressed steady-state grounding line ( $S = 0$ ) for  $\alpha > 0$  is locally unstable and occurs  
 463 at the critical thickness  $d_0$ , i.e. at the dimensionless ocean depth

$$\beta_0 = d_0(1 - \delta) \approx 2.11. \quad (4.1)$$

464 If  $\beta < \beta_0$ , an unstable steady state for  $S = 0$  therefore occurs at the position  $x_G =$   
 465  $(\beta - \beta_0)/\alpha$ . If instead  $\beta > \beta_0$ , no such steady state exists and, in accordance with the  
 466 prediction of (3.4) that  $V < 0$  if  $|b| > \beta_0$ , an unbuttressed grounding line would retreat  
 467 unconditionally. Thus, the form of the stability diagram differs qualitatively depending  
 468 on whether  $\beta$  is greater than or less than  $\beta_0$ .

469 4.2.1. The case  $\beta/\beta_0 < 1$ 

470 Beginning with the case  $\beta/\beta_0 < 1$ , I show the continuous variation of the stability  
 471 diagram with  $S$  constructed for  $\alpha = 2 \times 10^{-3}$ ,  $\beta = 1.4 < \beta_0$  and  $x_C = 0$  in figure 4.  
 472 The initial effect of introducing lateral stresses is to cause the unstable steady state to  
 473 move upstream. This produces a more secure ice-sheet configuration because a grounding  
 474 line must be displaced further upstream in order for runaway retreat to trigger. The  
 475 hysteresis effect discussed previously in the unbuttressed context (Schoof 2007a) can  
 476 therefore apply to a buttressed grounding line. However, the grounding line must be  
 477 displaced further upstream in order for positive-feedback retreat to instigate. At the  
 478 critical drag parameter  $S_* \approx 6.9 \times 10^{-4}$ , secondary grounding abruptly invalidates the  
 479 consistency of the unstable steady state predicted by (3.1). The region in which secondary  
 480 grounding is predicted in steady state is shown as a dark green region outlined by a thick  
 481 dotted curve. The invalidated steady-state solution to (3.1) is shown as a thin dotted  
 482 curve extended into this region. For  $S < S_*$ , collapse of the ice sheet occurs conditionally  
 483 on the grounding-line position lying upstream of the unstable steady state (similarly to  
 484 the unbuttressed case,  $S = 0$ ). For  $S > S_*$ , the question of grounding-line migration is  
 485 complicated fundamentally by the potential interference of secondary grounding. For the  
 486 case of negative bed slope considered above, the qualitative effect of secondary grounding  
 487 on the direction of grounding-line migration was not a point of uncertainty because  
 488 secondary grounding simply reinforces the prediction of advance already indicated by  
 489 the stability variable,  $V > 0$ . In the present case, secondary grounding instead covers  
 490 a considerable region for which the stability variable predicts retreat ( $V < 0$ ) and it is  
 491 therefore possible – in principle – for secondary grounding to suppress the grounding-line  
 492 retreat that would occur in this situation if the ice shelf was to remain fully floating.

493 To investigate the possible interference of secondary grounding, I conducted time-  
 494 dependent numerical calculations of the full equations (2.17)–(2.21) for values of  $S$  which  
 495 straddle the two side of the critical threshold  $S_*$ . The Lagrangian numerical scheme ap-  
 496 plied is detailed in Pegler (2018). The computations were initialised using fully developed  
 497 grounded and floating regions represented by the uniform-flux solutions to (2.17). The  
 498 ice-divide position is chosen as  $x_D = -3^3$ . For  $S > S_*$ , the secondary grounding implies  
 499 that the steady-state ice shelf produced at this position would intersect the bedrock; for  
 500 these cases, I initialised the shelf using the steady-state profile (derived in Pegler (2016)  
 501 and reviewed by (5.1) in Pegler (2018)) clipped along the bedrock, leaving a shallow gap  
 502 initially between the base of the ice shelf and the bedrock.

503 As a benchmark, I first consider the marginally subcritical value of  $S = 6.5 \times 10^{-4} < S_*$ ,  
 504 for which secondary grounding is *not* predicted in steady state, and corroborate the di-  
 505 rection of grounding-line migration predicted by the sign of the stability variable (3.3).  
 506 The evolutions of a grounding line initiated just upstream and just downstream of the  
 507 unstable state are shown in figure 5(a). These initial positions are indicated by crosses in  
 508 figure 4. The evolutions confirm the onset of a continuous advance or retreat, thus verify-  
 509 ing the direction of grounding-line migration predicted by the sign of  $V$ . The results show  
 510 that a buttressed grounding line will undergo runaway tipped retreat if the buttressing  
 511 is insufficient to outweigh the destabilising effect of buoyancy. An apparent oscillation in  
 512  $x_G(t)$  for the retreating example represents some periodic secondary contacts between  
 513 the ice shelf and the bedrock. Despite these contacts, collapse of the ice sheet ultimately  
 514 occurs.

515 Next, I consider the marginally supercritical value  $S = 7.5 \times 10^{-4} > S_*$ . The grounding-  
 516 line evolution for this example is shown in figure 5(b). Here, I initiated the grounding  
 517 line far upstream into the (dark green) region where retreat is predicted in the absence

16

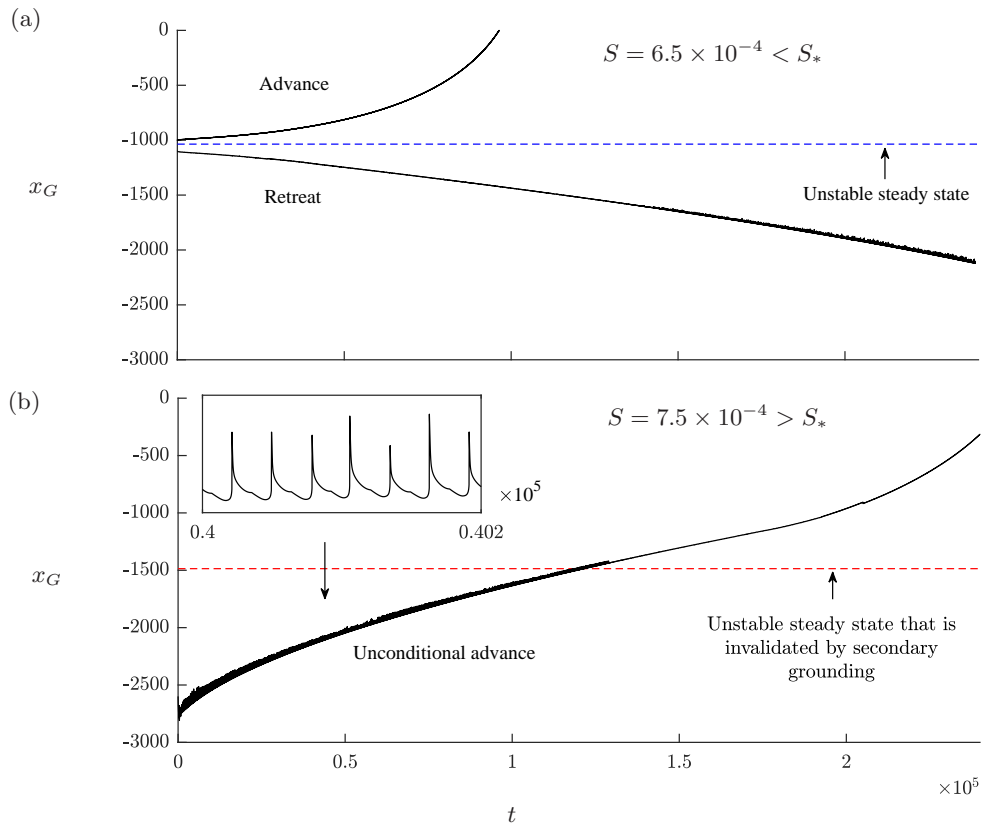
*S. S. Pegler*

FIGURE 5. Grounding-line evolutions  $x_G(t)$  predicted by the numerical solution to (2.17)–(2.21) for the positive bed slope  $\alpha = 2 \times 10^{-3}$ , reference ocean depth  $\beta = 1.4$ , ice-divide position  $x_D = -3000$ , and (a) a subcritical drag parameter  $S = 6.5 \times 10^{-4} < S_*$  and (b) the slightly larger, supercritical value  $S = 7.5 \times 10^{-4} > S_*$ . The evolutions in (a) illustrate advance and retreat either side of the unstable steady state, confirming the direction of migration predicted by the stability variable (3.3). For (b), the grounding line is initialised deeply into the region where the stability variable (3.3) predicts retreat,  $V < 0$ . Nevertheless, a net advance of the grounding line occurs as a consequence the additional buttressing generated by basal stresses in a ‘marginal-flotation zone’ in front of the grounding line. The intermittent ‘grazing’ between the ice shelf and the bedrock in this region produces an oscillation in  $x_G(t)$ , which is illustrated by the enlargement in the inset of (b).

518 of secondary grounding,  $V < 0$ , at  $x_G(0) = -2.6 \times 10^3$  (shown as a plus sign in figure  
 519 4). In direct contradiction to the sign of  $V$ , the grounding line undergoes a persistent  
 520 net advancement. This conclusion stands in remarkable contrast to the runaway retreat  
 521 occurring for the slightly smaller, marginally subcritical value  $S = 6.5 \times 10^{-4}$  shown in  
 522 figure 5(a). The retreat is suppressed by added buttressing generated by intermittent con-  
 523 tacts between the ice shelf and the bedrock; the periodic surges in the buttressing force  
 524 generated by the contacts produces the oscillation in  $x_G(t)$  shown in the inset of figure  
 525 5(b). The prediction of secondary grounding in steady state therefore overrides the pre-  
 526 diction of grounding-line retreat indicated by the sign of the stability variable (3.3), with  
 527 the result of unconditional advance. The buttressing arising from lateral stresses alone,  
 528 as predicted by (3.2b) and assumed in evaluating (3.3), considerably underestimates the

529 effective buttressing force generated over time as a consequence of intermittent grounding  
 530 of localised sections of the ice shelf over an extended region in front of the grounding  
 531 line. The criterion for secondary grounding,  $S > S_*(\alpha, \beta)$ , creates a sharp threshold  
 532 separating conditions producing runaway grounding-line retreat from those resulting in  
 533 unconditional advance. The hysteresis effect possible for  $S < S_*$  is thereby eliminated,  
 534 leading to complete suppression of grounding-line retreat.

#### 535 4.2.2. The marginal-flotation regime

536 The intermittent contacts between the ice shelf and the bedrock produce a distinctive  
 537 flow regime referred to as ‘marginal flotation’. The regime is characterised by slight  
 538 modulations in thickness that produce temporarily grounded regions over a well-defined  
 539 interval intermediate to the fully grounded and fully floating regions. The overall structure  
 540 of the flow is illustrated in figure 6(a). Here, the grounded regions are shown by  
 541 blue shading, illustrating the firmly grounded region upstream, as well as a patch of  
 542 temporarily grounded ice further downstream. A plot of  $H(x, t) - d(x)$  in figure 6(b)  
 543 clearly indicates the three-component structure of the ice sheet. A fully grounded region  
 544 upstream, wherein  $H > d$ , a fully floating region downstream, wherein  $H < d$ , and an  
 545 intermediate zone in which the thickness straddles the flotation thickness,

$$H \approx d(x) \quad (\text{marginal flotation}). \quad (4.2)$$

546 This region is referred to as the ‘marginal-flotation zone’.

547 The marginal-flotation zone represents a tertiary component of a marine ice sheet, additional  
 548 to the fully grounded and fully floating regions. In essence, it replaces the notion  
 549 of a grounding line to a grounding *area* in which the transition between floating and  
 550 grounded regions takes place over an extended region. It is possible that certain regions  
 551 of the WAIS may lie in this marginal-flotation state, which may appear as distributed  
 552 grounding zones or ice planes. Since the present-day WAIS is likely to be in a state of  
 553 decline, such regions may not be widespread; as noted above, the development of this  
 554 region is a hallmark of a grounding line recovering from tipped retreat. However, the  
 555 prediction is a fundamental feature of ice-sheet dynamics that may be important in understanding  
 556 their formation on time scales of glaciation and potential to recover following  
 557 destabilisation.

558 The patterns of grounding and detachment in the marginal-flotation zone, as predicted  
 559 by the numerical solution, take the form of travelling waves, which begin at the downstream  
 560 end of the marginal-flotation zone and propagate to the ‘primary’ grounding line  
 561 at the upstream end of the marginal-flotation zone. The merging events of the grounded  
 562 wave to the fully grounded region at the primary grounding line produce the oscillations  
 563 shown in figure 5(b). The phenomenon of intermittent grounding represents a remarkable  
 564 feature of the model, namely, that once the interior of the ice shelf grounds, the switch  
 565 in the governing equation (2.17) leads to a new force balance that immediately favours  
 566 its detachment from the base. Reducing the time step was thus found to increase the  
 567 frequency of the switches and hence the frequency of the grounded pulses. Nonetheless,  
 568 the time-averaged predictions of the model (averaged over a few periods of the numerical  
 569 oscillation, for example) is unchanged to leading-order in small time step, indicating that  
 570 the long-term migration predicted is physically meaningful.

571 In order to investigate the structure of the marginal-flotation zone, I evaluate the  
 572 time-averaged indicator function

$$Gr(x, t) = \frac{1}{2T} \int_{t-T}^{t+T} 1_{\{H(x, \tau) > d(x)\}} \, d\tau, \quad (4.3)$$

18

S. S. Pegler

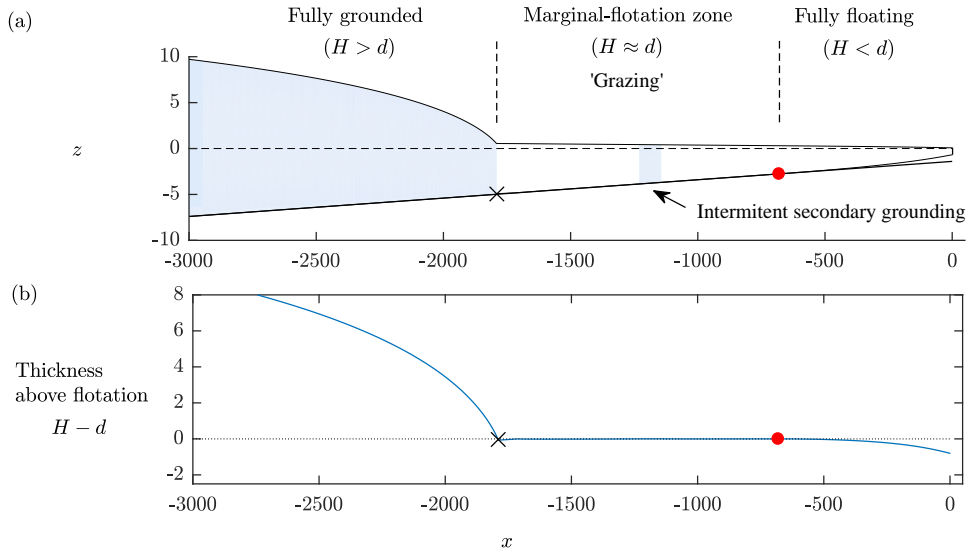


FIGURE 6. Panel (a) shows the three-component structure of a marine ice sheet, predicted by the numerical solution to the full system (2.17)–(2.21) for the example  $\alpha = 2 \times 10^{-3}$ ,  $\beta = 1.4$  and  $x_D = -3000$ , shown at time  $t = 7.5 \times 10^4$ . Grounded sections of the flow are shown shaded. Panel (b) shows the difference  $H(x, t) - d(x)$ , which distinguishes the three components of the marine ice sheet: the fully grounded region,  $H > d$ , the fully floating region,  $H < d$ , and, connecting them, the marginal-flotation zone, through which the thickness straddles the flotation thickness,  $H \approx d$ . The black cross and red circle mark the edges of the marginal-flotation zone.

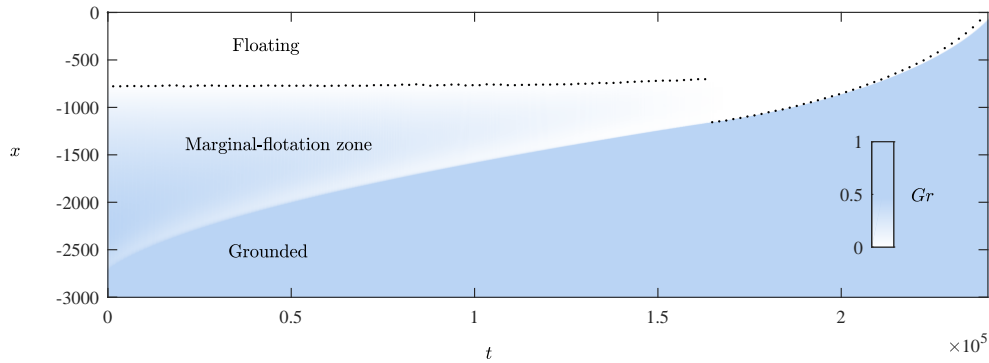


FIGURE 7. The evolution of the grounding number  $Gr(x, t)$  defined by (4.3), which measures the proportion of time that a region of the ice sheet lies grounded over a time scale of  $T = 500$ . The fully grounded region is represented by  $Gr = 1$ , the fully floating region by  $Gr = 0$ , and the marginal-flotation zone by  $0 < Gr < 1$ . The end of the marginal-flotation zone is illustrated by a dotted curve. The extent of the zone reduces over time until it vanishes at  $t \approx 1.65 \times 10^5$  to leave a sharp transition between fully grounded and fully floating regions. Surprisingly, the transition from floating to grounding does not occur monotonically, with a local minimum in  $Gr$  indicated by the relatively lighter band just downstream of the grounding line.

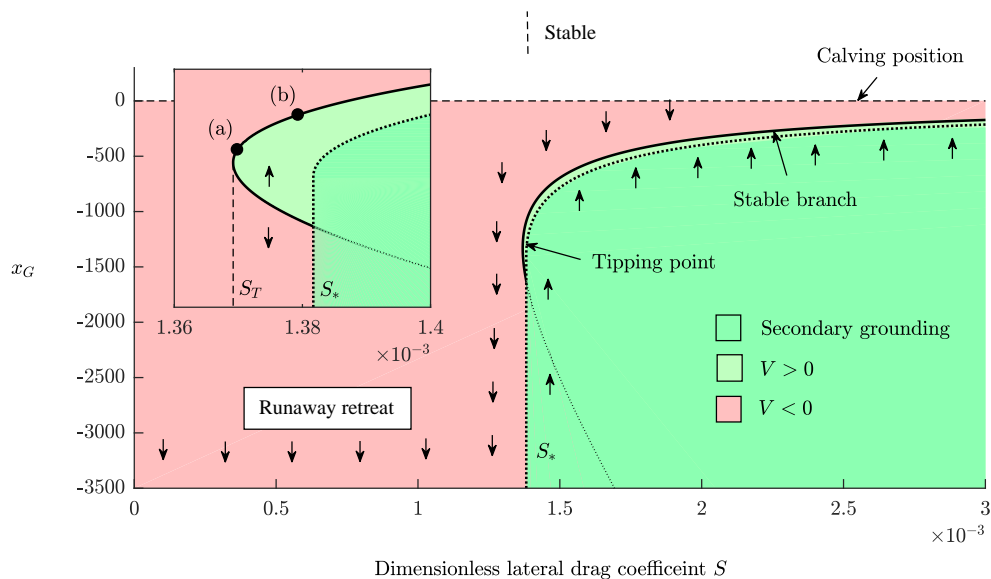


FIGURE 8. The stability diagram for the positive bed slope  $\alpha = 2 \times 10^{-3}$  and the reference ocean depth  $\beta = 2.8$  shown as a continuous variation of the drag parameter  $S$ . Colour indicates the value of the stability variable  $V(x)$  defined by (3.3) and the dark green region with a dashed outline represents the region of secondary grounding. Grounding-line retreat occurs unconditionally below a critical value  $S_T(\alpha, \beta) = 1.369 \times 10^{-3}$ . At  $S = S_T$ , two steady arise (one stable, the other unstable), as illustrated in the enlargement. The circular markers in this inset indicate the initial grounding-line positions for the computations following ice-shelf collapse of figure 9. At the slightly larger value  $S_*(\alpha, \beta) = 1.382 \times 10^{-3}$ , secondary grounding invalidates the unstable steady state and suppresses the possibility of runaway grounding-line retreat. Above  $S_*$ , unconditional stabilisation towards the steady state occurs.

573 where the integrand is equal to unity if the ice sheet is grounded and zero if it is floating,  
 574 and  $T$  is a specified time scale assumed smaller than the time scales on which the primary  
 575 grounding line migrates. The variable  $Gr(x, t)$  quantifies the proportion of time that a  
 576 given point on the ice sheet lies grounded over the time interval  $[t - T, t + T]$ . For a fully  
 577 grounded or floating region,  $Gr$  equals unity and zero, respectively, and intermediate  
 578 values represent marginal flotation. The value of  $Gr(x, t)$  is shown as a density plot  
 579 in figure 7(a) for the example of figure 5(b) and  $T = 500$ . The plot shows that the  
 580 upstream boundary of the marginal-flotation zone, i.e. the ‘primary’ grounding line,  
 581 gradually advances while the downstream boundary remains approximately constant.  
 582 Perhaps surprisingly, the transition from  $Gr = 1$  to 0 does not occur monotonically; there  
 583 is a band of relatively less grounding in front of the primary grounding line compared to  
 584 the interior of the marginal-flotation zone (this structure mirrors that of the thickness  
 585 profile of a confined ice shelf, which involves a region of rapid thinning in an extensional  
 586 boundary layer in front of the grounding line; Pegler 2016). The marginal-flotation zone  
 587 vanishes at  $t = 6.5 \times 10^4$ , with a sharp transition between the fully grounded and floating  
 588 regions persisting subsequently.

#### 589 4.2.3. The case $\beta/\beta_0 > 1$

590 I now address the qualitatively different case  $\beta > \beta_0$ . The stability diagram for  
 591  $\alpha = 2 \times 10^{-3}$  and the deeper reference ocean depth  $\beta = 2.8 > \beta_0$  is shown in figure  
 592 8. In contrast to the case  $\beta < \beta_0$ , no steady state is possible if  $S = 0$ , in which case an

593 unbuttressed grounding-line would retreat unconditionally. As  $S$  is increased, this con-  
 594 clusion continues to hold up to a critical value  $S_T(\alpha, \beta) \approx 1.369 \times 10^{-3}$ , whereat two  
 595 steady states – one stable, the other unstable – appear at  $x_T \approx -1330$ . As  $S$  is increased  
 596 further, the stable state moves downstream and the unstable state moves upstream. At  
 597 a slightly larger value  $S_* = 1.382 \times 10^{-3}$ , secondary grounding abruptly invalidates the  
 598 unstable steady state, and completely covers the upstream region for which  $V < 0$ . A  
 599 single, stable steady state then remains. In regard to the contributions to the terms in  
 600 the numerator of (3.3), the critical value  $S_T$  represents the threshold at which the stabil-  
 601 ising effect of ice-shelf buttressing critically cancels the destabilising effects of buoyancy  
 602 and extensional stress, creating a new stable steady-state branch along the interior of a  
 603 positive bed slope.

604 The branch of stable steady states is a new property of the stability diagram compared  
 605 to  $\beta < \beta_0$  that is inherently associated with the stability mechanism generated by ice-  
 606 shelf buttressing. A conclusion from §4.2.1 illustrated in figure 4 is that there is no *stable*  
 607 steady state possible if  $\beta < \beta_0$  for all values of  $S$ . By contrast, the stable steady states  
 608 arising here for  $\beta > \beta_0$  and  $S > S_T$  are a robust long-term regime, indicating that the  
 609 removal of such states as a consequence of parameter variation (e.g. reduction of the  
 610 upstream flux  $Q$ ) provides the trigger to tipped retreat of a buttressed marine ice sheet.  
 611 A key question is: how might a runaway grounding-line retreat be triggered if a marine  
 612 ice sheet lies on the stable branch? One plausible trigger is the large-scale collapse of the  
 613 ice shelf, which abruptly removes the buttressing force, and may provoke instability if  
 614 the ice shelf fails to recover sufficiently quickly. Another mechanism for destabilisation  
 615 is for parameters, such as the calving position or melt rate, to vary in time and cause  
 616 a transition from supercriticality,  $S > S_T(\alpha, \beta)$ , to subcriticality,  $S < S_T(\alpha, \beta)$ . The  
 617 stability diagram of figure 8 indicates that such a transition would involve an initially  
 618 quasi-steady migration along the stable branch followed by a sudden onset of runaway  
 619 grounding-line retreat upstream of the critical ‘cliff edge’ grounding-line position  $x_T$ .

620 In order to investigate the first possibility of destabilisation from ice-shelf collapse, I  
 621 ran a series of time-dependent computations initialised at a selection of positions along  
 622 the stable branch. In each case, I removed the ice shelf completely at  $t = 0$ . Subsequently,  
 623 the front of the ice shelf was evolved with the flow rate until it recovered to the position  
 624  $x_C$ , beyond which time the calving front was again imposed at  $x_C$ . It was found that the  
 625 grounding line recovers in all cases, with the exception of a range of  $S$  *very* close to the  
 626 critical value  $S_T \approx 1.369$ . The results for two marginally supercritical critical values of  
 627  $S$  given by  $S = 1.370 \times 10^{-3}$  and  $1.380 \times 10^{-3}$  are illustrated in panels (a) and (b) of  
 628 figure 9, respectively. For case (a), the removal of the ice shelf leads to a relatively sudden  
 629 retreat of the grounding line to a minimum position at  $t \approx 1500$ . Near this minimum,  
 630 the front of the ice shelf reaches its former calving position, indicated by a filled circular  
 631 marker. Following this, the grounding line remains upstream of the unstable steady state  
 632 and long-term recovery fails. For case (b), the initial retreat of the grounding line instead  
 633 remains downstream of the unstable steady state indicated by a dashed line, which is  
 634 consistent with a long-term recovery to the original steady state. It should be noted that  
 635 the range of values of  $S$  for which recovery fails is extremely limited to situations very  
 636 close to  $S_T$ : all values of  $S > 1.001 S_T$  undergo a complete recovery.

637 In light of the results above, I hypothesise that the destabilisation of a marine ice  
 638 sheet from a buttressed steady state is more likely to arise from *parametric* variation  
 639 in the properties of the ice sheet inducing a transition from supercriticality  $S > S_T$   
 640 to subcriticality  $S < S_T$ . This transition has the character of a ‘cliff-edge’, with robust  
 641 stability occurring for  $S > S_T$  to a sudden loss of stability occurring for  $S < S_T$ .  
 642 To illustrate this mode of destabilisation, I ran a computation in which the parameter



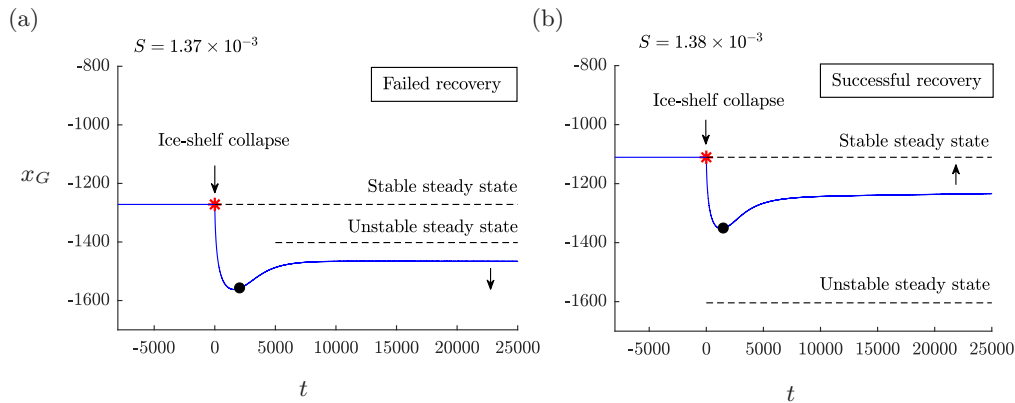


FIGURE 9. Grounding-line evolutions following the collapse of the ice shelf for  $\alpha = 2 \times 10^{-3}$ ,  $\beta = 2.8$  and  $x_D = -3 \times 10^3$  for (a)  $S = 1.37 \times 10^{-4}$  and (b)  $S = 1.38 \times 10^{-4}$ , obtained from the numerical solution of the full equations (2.17)–(2.21). Each computation is initialised from the corresponding stable steady state, corresponding to the positions of the circular markers in the inset of figure 8. In case (a), the grounding line initially retreats upstream of the unstable steady state and ultimately fails to recover to the original steady state. The time at which the front of the ice shelf reaches its former calving position,  $x_G(t) = 0$ , is indicated by a filled circle. In case (b), the grounding line instead remains downstream of the unstable steady state and a long-term recovery ensues. The results show that an ice-shelf collapse generally leads to total restoration of the marine ice sheet for even marginally supercritical values of  $S > S_*$ .

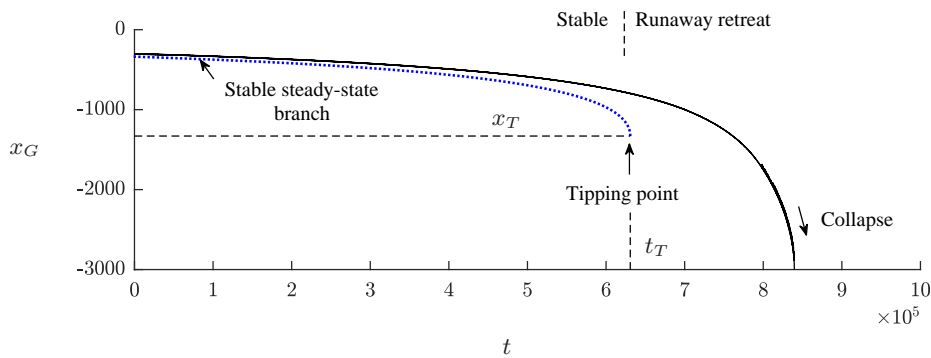


FIGURE 10. The grounding-line evolution  $x_G(t)$  following initialisation at the stable steady state for  $S = S_0 = 2 \times 10^{-3} > S_T$ ,  $\alpha = 2 \times 10^{-3}$ ,  $\beta = 2.8$ , and  $x_D = -3 \times 10^3$  and a gradual ramping down of the lateral drag parameter  $S = S(t)$  to the subcritical value  $S = 10^{-3} < S_T$  linearly over a time scale of  $t = 10^6$ . The plot illustrates the initial quasi-steady migration along the stable branch given by the solution to (3.1) shown as a dotted blue curve, followed by the onset of a runaway grounding-line retreat beyond the ‘cliff-edge’ at which the steady branch terminates. The critical transition to instability occurs once  $S(t) > S_T \approx 1.36 \times 10^{-3}$  or  $t > t_T \approx 6.3 \times 10^5$ .

643  $S = S(t)$  is ramped down linearly from the supercritical value  $S = 2 \times 10^{-3} > S_T$  to the  
 644 subcritical value  $10^{-3} < S_T$  over a time scale of  $t = 10^6$ , shown in figure 10. Initially,  
 645 the grounding line retreats in proximity to the stable branch of steady states shown by  
 646 a blue dotted curve in a quasi-steady manner, representing ‘stable’ retreat. Once the  
 647 threshold  $S_T$  is passed at  $t = t_T \approx 6.3 \times 10^5$ , a relatively rapid ‘tipped’ grounding-line  
 648 retreat ensues, culminating in detachment of the ice sheet a relatively short time later at  
 649  $t \approx 8.4 \times 10^5$  whereat  $x_G = x_D$ . More than 80% of the retreat with respect to the initial

position occurs for  $t > t_T$ , confirming that the critical value  $S_T$  represents a tipping point. Thus, while the ice sheet is totally secure for even marginally supercritical values of  $S > S_T$  (against even a full ice-shelf collapse), security vanishes completely below the threshold  $S_T$ .

## 5. Thresholds for tipping and recovery of a marine ice sheet

The general conditions for stability of a marine ice sheet on a retrograde slope are shown in figure 11. Here, I plot the critical dimensionless lateral drag coefficients,  $S_*(\alpha, \beta)$  and  $S_T(\alpha, \beta)$ , for the illustrative case  $\alpha = 2 \times 10^{-3}$  as a function of  $\beta$ , which provide the critical boundaries of the possible regimes. For  $S > S_T$ , the inducement of secondary grounding guarantees the stability of the ice sheet (the green region). For  $S < S_*$ , secondary grounding cannot suppress the retreat, and the stability depends on the dimensionless ocean depth  $\beta$ . In this case, if  $\beta < \beta_0 \equiv (1 - \delta)d_0$  (the yellow region), runaway grounding-line retreat occurs if and only if the grounding line lies upstream of the unstable steady state. For  $\beta > \beta_0$ , runaway grounding-line retreat is guaranteed (the red region) with the exception of a very narrow band  $S_T < S < S_*$  of values where retreat is conditional on the grounding line lying upstream of the unstable steady state. The plot shows that the transition to tipped retreat from a buttressed steady state generally occurs abruptly across a parametric threshold. For the unbuttressed case, a transition to runaway retreat can occur only if  $\beta$  changes from less than  $\beta_0$  to greater than  $\beta_0$ . A transition from buttressed stability also depends on a transition from  $S > S_T$  to  $S < S_T$ , representing a stability criterion that is entirely distinct from the transition associated with unbuttressed MISI. Subsequent recovery of the grounding line depends on  $S$  increasing to the slightly larger value  $S_* \gtrsim S_T$ .

For a general topography  $b(x)$  and calving position, the ‘tipping point’ critical values of  $S$  can be defined by the functionals

$$S_T[b, x_C] \equiv \min_x \{S : (3.1) \text{ holds}\}. \quad (5.1)$$

$$S_*[b, x_C] \equiv \min_x \{S : (3.5) \text{ holds}\}. \quad (5.2)$$

These represent the minimum value of  $S$  for which a stable steady state exists, and the minimum value of  $S$  such that secondary grounding occurs in steady state, respectively. The stability of the ice sheet is critically removed once  $S$  drops below  $S_T$ . In practise, it is possible for there to be multiple localised tipping points (each a saddle-node bifurcation), and these will be illustrated by the stability diagram constructed for a given scenario. In such cases, transitioning across a tipping point may cause the grounding line to migrate to a new steady state upstream. The value of (5.1) represents the final tipping point below which the system will continue to retreat without subsequently stabilising towards a new steady state.

The plot of figure 11 indicates that the two critical values  $S_T$  and  $S_*$  are numerically almost coincident. This coincidence occurs because both values approximate the location where the universal profile of the ice shelf intersects the bedrock (Pegler 2018). In order to confirm that  $S_*$  and  $S_T$  are approximately coincident in general, I plot these functions for a range of bed slopes  $\alpha = 2 \times 10^{-4}, 2 \times 10^{-3}, 2 \times 10^{-2}$ , in figure 12 (spanning three orders of magnitude). The plot shows that  $S_T$  (solid) and  $S_*$  (dotted) practically coincide in each case. Note that  $S_T$  is only defined for  $\beta > \beta_0$  because it represents the critical turning point of the branch of stable steady states, which only exists for  $\beta > \beta_0$ .

It should be noted that there is a special region of the parameter space,  $S < S_0(\beta)$ , for which the calving front of the ice shelf itself is predicted to penetrate the bedrock

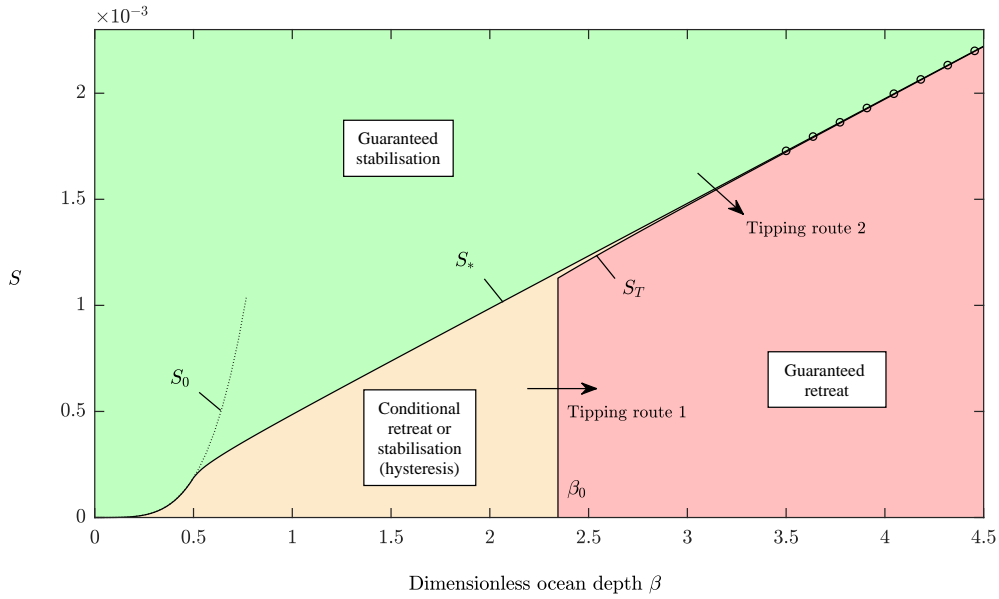


FIGURE 11. Regime diagram illustrating the conditions for stability of a buttressed marine ice sheet on a retrograde slope across the space of dimensionless reference ocean depth  $\beta$  and lateral drag coefficient  $S$ . The dimensionless slope  $\alpha = 2 \times 10^{-3}$  is illustrated, and is representative of the general case. If  $S > S_*$  (green), the system is guaranteed to remain stable for any dimensionless ocean depth. If  $S < S_*$  and  $\beta < \beta_0 \approx 2.345$  then stabilisation is contingent on whether the grounding line lies downstream of the unstable steady state (yellow). If  $S < S_*$  and  $\beta > \beta_0$  then there is a very narrow range  $S_T < S < S_*$  for which stability is also contingent on the grounding line lying downstream of the unstable steady state (yellow). Otherwise, runaway grounding-line retreat is guaranteed (red). The approximation for the critical tipping-point value of  $S_*$  given by (5.5) is shown as a line of circular markers. The critical value of  $S_0$  given by (5.3) for which the calving front is predicted to contact the bedrock for  $S < S_0$  is shown as a dotted black curve. The arrows indicate the two different pathways for instigation of instability, as given by the two criteria (5.7) and (5.8).

692 (as opposed to the interior to the ice shelf). For these special situations, the critical  
 693 cotangency conditions for secondary grounding (3.5) are not applicable and, instead, the  
 694 condition for secondary grounding is  $H_C > \beta$ . Using the analytical prediction for the  
 695 calving-front thickness for  $n = 1$ , namely,  $H_C = \kappa(S/\delta^2)^{1/4}$ , where  $\kappa \approx 1.502$  (Pegler  
 696 2016), I determine this critical value as

$$S_0 = \delta^2 \{ \beta / [\kappa(1 - \delta)] \}^4, \quad (5.3)$$

697 which is shown by the thin dotted curves in figures 11 and 12. The value  $S_0$  represents  
 698 the termination of the threshold value  $S_*$  for which cotangency is possible, as illustrated  
 699 figure 12.

700 To gain analytical insight into the nature of the buttressed stability criterion  $S >$   
 701  $S_*(\alpha, \beta)$ , and its parametric form, I determine an analytical approximation for  $S_*(\alpha, \beta)$ .  
 702 As discussed in Pegler (2018), the critical cotangency condition for secondary grounding  
 703 (3.5) is given approximately by the strong-buttressing limiting balance of (3.1), namely,

$$\frac{1}{2} \delta d(x_G)^2 \approx B(x_G, x_C). \quad (5.4)$$

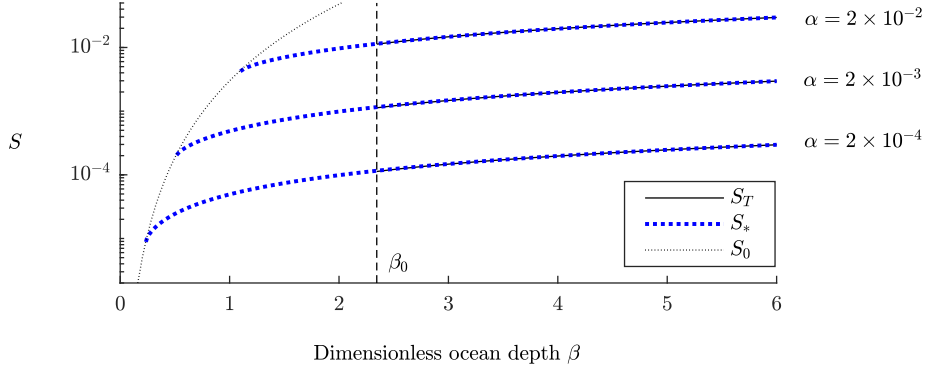


FIGURE 12. The critical values of the dimensionless lateral shear drag coefficients,  $S_T$  (solid black curve) and  $S_*$  (dotted blue curve), representing the terminus of the stable branch of steady states and of the instance of secondary grounding, respectively, plotted against the reference ocean depth  $\beta$  for bed slopes  $\alpha = 2 \times 10^{-4}$ ,  $2 \times 10^{-3}$  and  $2 \times 10^{-2}$ , spanning two orders of magnitude. The plot illustrates the approximate equivalence of  $S_T$  and  $S_*$  across the complete parameter space. The critical dimensionless ocean depth  $\beta_0$  for which the stable branch exists for  $\beta > \beta_0$  is shown as a vertical dashed line. The critical drag coefficient  $S_0$  for which the calving front of the ice shelf is predicted to contact the bedrock is shown as a thin dotted curve, and provides the minimum of  $S_*$  for each value of  $\alpha$ .

Substituting (3.2b) into (5.4), and rearranging for  $S$ , I determine the threshold value

$$S_* \approx \min_x \left[ \frac{1}{2} \delta d(x)^2 / (x_C - x) \right], \quad (5.5)$$

$$= 2\delta(1 - \delta)^{-2} \alpha \beta \quad (5.6)$$

704 for the linear bedrock. The analytical approximation (5.6) is shown as a line of circular  
 705 markers in figure 11 and is confirmed to provide excellent agreement with the numerical  
 706 result. The result implies a near linear relationship between  $S_*$  and the basal slope  $\alpha$  and  
 707 the reference depth  $\beta$ .

The result of (5.6) yields an analytical condition for grounding-line stability,  $S < S_*(\alpha, \beta)$ . A transition to tipped retreat will therefore occur, for example, if the flux  $Q$  reduces sufficiently for the threshold  $S = S_*$  to become crossed. In discussing the critical transitions from a stable ice sheet to tipped retreat, I henceforth assume that the topography downstream of the reference position  $x = 0$  slopes downwards, such that there is a topographic maximum at  $x = 0$  and  $\beta$  is the minimum ocean depth. For the context of an unbuttressed grounding line, a transition from a stable configuration on the downwards slope for  $x > 0$  to a positive slope for  $x < 0$  occurs critically once the dimensionless reference depth  $\beta$  drops below the value  $\beta_0$ . In the general buttressed context, there are instead *two* distinct criteria necessary to trigger instability in this configuration, namely, both  $\beta > \beta_0$  and  $S < S_T$ . In their dimensional forms, these criteria read

$$Q < \frac{\rho g}{\mu_0} \left[ \frac{\delta \mu_0}{8C_-} \left( \frac{|b_0|}{1 - \delta} \right)^5 \right]^{\frac{1}{2}} \quad (\text{tipping criterion 1}), \quad (5.7)$$

$$Q < \frac{2\rho g' a |b_0| w}{(1 - \delta)^2 C_+} \quad (\text{tipping criterion 2}), \quad (5.8)$$

708 respectively. These two distinct necessary criteria for transitioning to tipped grounding-

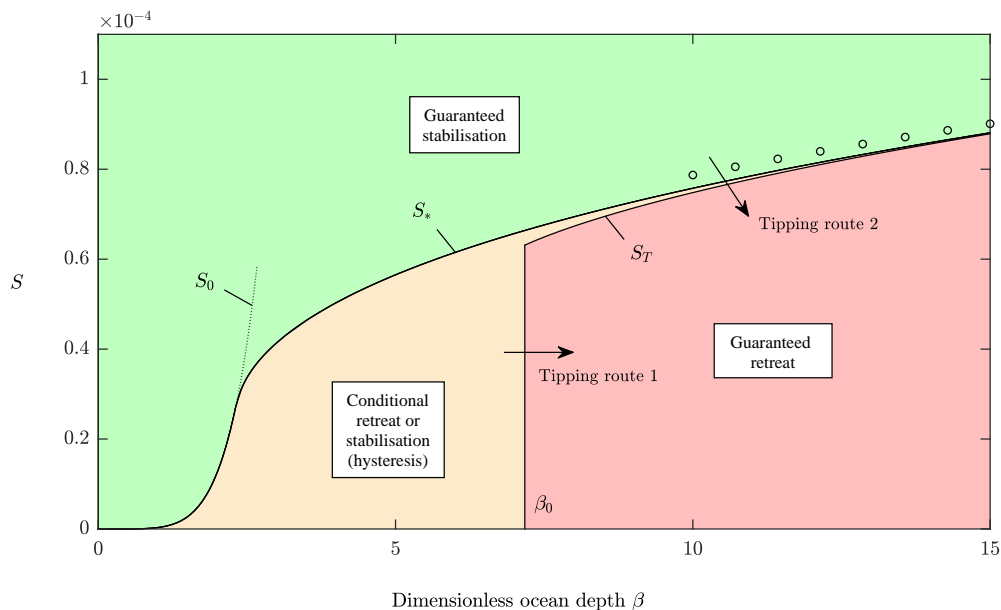


FIGURE 13. Regime diagram illustrating the conditions for stability of a buttressed marine ice sheet on a retrograde slope across the space of dimensionless reference ocean depth  $\beta$  and lateral drag coefficient  $S$  for the power-law case  $n = 3$ . The diagram is the power-law analogue of figure 11. The dimensionless slope  $\alpha = 2 \times 10^{-4}$  is illustrated, and is representative of the general case. If  $S > S_*$  (green), the system is guaranteed to remain stable for any dimensionless ocean depth. If  $S < S_*$  and  $\beta < \beta_0 \approx 2.345$  then stabilisation is contingent on whether the grounding line lies downstream of the unstable steady state (yellow). If  $S < S_*$  and  $\beta > \beta_0$  then there is a very narrow range  $S_T < S < S_*$  for which stability is also contingent on the grounding line lying downstream of the unstable steady state (yellow). Otherwise, runaway grounding-line retreat is guaranteed (red). The approximation for the critical tipping-point value of  $S_*$  given by (6.4) is shown as a line of circular markers. The critical value of  $S_0$  given by (6.3) for which the calving front is predicted to contact the bedrock for  $S < S_0$  is shown as a dotted black curve.

709 line retreat are illustrated by the arrows in the regime diagram of figure 11. Importantly,  
 710 either one can provide the critical threshold for tipping, and each represents a different  
 711 pathway in parameter space resulting in runaway retreat. For an unbuttressed grounding  
 712 line,  $\lambda_+ = \infty$  and criterion 2 is automatically satisfied. The only criterion for transition  
 713 to instability is then criterion 1, which represents the threshold at which the thickness  
 714 necessary for an unbuttressed steady-state grounding line to exist decreases below the  
 715 minimum flotation thickness  $|b_0|$ . Criterion 2 introduces a distinct threshold representing  
 716 the condition for the destabilising effect of buoyancy to critically outweigh the stabilising  
 717 effect of ice-shelf buttressing. It is interesting that for  $S < S_*(\beta_0)$ , only criterion 1 is  
 718 necessary for tipping. Over this region of the parameter space, the buttressing force,  
 719 while present, therefore plays no role in controlling the onset of tipping.

## 720 6. Tipping thresholds controlled by ice-shelf calving and melting

721 To this point, I have illustrated the onset of tipped retreat by variation of the di-  
 722 mensionless lateral shear drag coefficient  $S$ , a parameter grouping that is dependent in  
 723 particular on snowfall accumulation  $Q$  and channel width. Here, I will demonstrate other  
 724 natural modes of transitioning to tipped retreat, namely, the retreat of the calving front

of the ice shelf  $x_C$  and an increase in the net rate of melting along the base of the ice shelf,  $-f(x)$ , which will each erode the buttressing force generated by the ice shelf. The dynamics of a grounding line is, via the buttressing force, sensitive to both the melt-rate distribution and the control of its calving position (e.g. Dupont & Alley 2005; Gagliardini *et al.* 2010; Nick *et al.* 2010; Gudmundsson *et al.* 2012; Gudmundsson 2013; Favier *et al.* 2014; Schoof *et al.* 2017). In particular, the possibility of a stable grounding line on a retrograde slope depends sensitively on the choice of calving model and its underlying parameters (Schoof *et al.* 2017).

For illustrating the critical tipping points associated with changes in calving position and melt rate, I will first confirm that the same qualitative features of the stability-regime diagram of figure 11 also apply for the shear-thinning power-law exponent  $n = 3$ . Thus, I write the expressions for  $E$  and  $B$  given by (2.10) and (2.11), which take the dimensionless forms

$$E[d(x_G)] = 4d(x_G)^{(n^2-3n-1)/n^2}, \quad (6.1)$$

$$B(x_G) = \frac{\delta}{2} \left\{ \left[ \frac{N}{\delta} \int_{x_G}^{x_C} S q(x')^{1/n} dx' + H_C^N \right]^{2/N} - H_C^2 \right\}, \quad (6.2)$$

where  $N \equiv (n+1)/n$ ,  $\tilde{H}_C \approx \kappa\eta$ ,  $\eta \equiv \delta^{-1/N} S^{1/(nN^2)}$ ,  $q = 1 - \int_{x_G}^x M(x) dx$ ,  $M(x) \equiv -f(x)\mathcal{L}/Q$  is the dimensionless melt-rate distribution, and I have again neglected the contribution due to  $db/dx$  in  $E$ .

The regime diagram constructed for  $n = 3$ ,  $\alpha = 2 \times 10^{-4}$ , zero melting  $M = 0$  and  $x_C = 0$  is shown in figure 13. The plot represents the power-law analogue of figure 11. As in the Newtonian case, there is a range of shallow slopes for which  $S < S_0(\beta)$ , where

$$S_0(\beta) = \delta^{n+1} (\beta/[\kappa(1-\delta)])^{nN^2}, \quad (6.3)$$

for which the calving front itself is predicted to intersect the bedrock. The regime diagram again shows the near coincidence of the critical values  $S_*$  and  $S_T$ . One difference compared to  $n = 1$  is that the critical values increase nonlinearly with  $\beta$ . Repeating the analysis used to develop (5.6), one can determine the approximation

$$S_*(\alpha, \beta) \approx \frac{\delta\alpha}{1-\delta} \left[ \frac{(n+1)\beta}{1-\delta} \right]^{\frac{1}{n}} \quad (6.4)$$

which is shown as a curve of circular markers in figure 13, confirming the nonlinear dependence.

To illustrate the control of stability by the calving position  $x_C$ , I show the stability diagram for  $\alpha = 2 \times 10^{-4}$  and  $S = 10^{-4}$  against a continuous variation of  $x_C$  in figure 14(a). In qualitative similarity to the stability diagrams shown with respect to the drag coefficient  $S$  (cf. figure 8), there is a stable steady-state branch above a critical value,  $x_C > x_{CT}$ . The plot illustrates the retreat of the grounding line induced by retreat of the calving front, and its eventual destabilisation below the critical calving position  $x_C = x_{CT}$ . Thus, if progressive retreat of the calving front occurs, there is an initial retreat of the grounding line along the stable branch before runaway grounding-line retreat triggers critically the calving front retreats upstream of the critical position  $x_{CT}$  interior to the retrograde slope. It is interesting to note that the conditions for tipping and recovery for this example of calving-induced tipping are almost coincident. The condition to lose a steady state is essentially the same as the condition for the ice shelf to reground. Consequently, recovery will essentially occur following parametric restoration. The hysteresis effects noted to apply for unbuttressed grounding lines (Schoof 2007a)

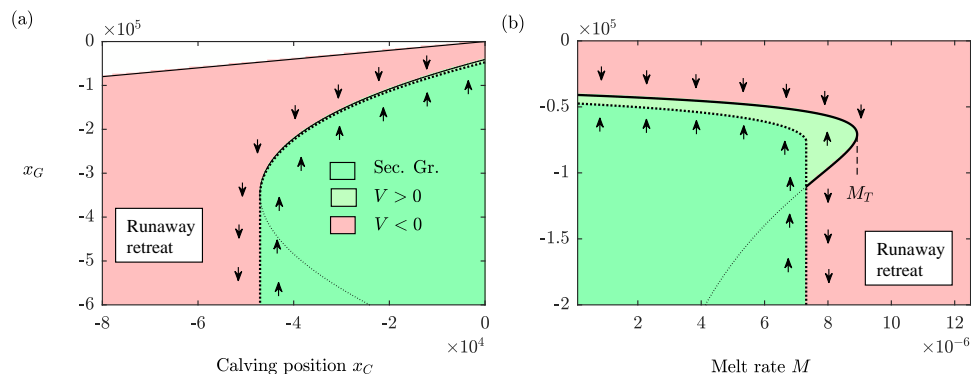


FIGURE 14. stability diagrams illustrating the grounding-line position and critical transition to instability against (a) calving position  $x_C$  and (b) melt rate  $M$ . For these examples,  $\alpha = 2 \times 10^{-4}$ ,  $\beta = 12$  and  $S = \times 10^{-4}$ . For (a), the melt rate  $M = 0$ . For (b), the calving position is  $x_C = 0$ .

759 therefore practically do not occur here. It should be noted that the results here are for a  
 760 prescribed calving position  $x_C$ . For a thickness-dependent calving law (e.g. Schoof *et al.*  
 761 2017),  $x_C$  can be treated as an unknown and its prescription replaced by imposition of the  
 762 implicit condition  $H(x_C) = H_C$ . In this case, the conditions for tipping are likely highly  
 763 sensitive to the parameter  $H_C$ , and this could be illustrated by a bifurcation diagram  
 764 constructed for this case.

765 To demonstrate the destabilisation as a consequence of increased melting, I plot the  
 766 stability diagram with respect to the dimensionless melt rate  $M$  in figure 14(b), which  
 767 is assumed to take a uniform value along the ice shelf for this example. The plot shows  
 768 a critical melt rate  $M_T$  above which destabilisation of the grounding line occurs. Inter-  
 769 estingly, the steady-state position of the grounding line stays relatively insensitive to the  
 770 melt rate along the entire stable branch. This indicates the potential for a more abrupt  
 771 transition to tipped retreat in situations where the destabilisation is induced primarily  
 772 by increasing melt-rate. The critical melt rate below which secondary grounding occurs,  
 773  $M_*$ , is also appreciably smaller than the critical value  $M_T$  representing the termination  
 774 of the steady-state branch. Based on a comparison between this stability diagram and  
 775 that obtained for calving-induced tipping (figure 14(a)), it is indicated that hysteresis  
 776 is more plausible for melt-induced tipping. That is, a grounding-line retreat stimulated by  
 777 melting may be relatively harder to reverse compared to a retreat triggered by calving.  
 778 This difference can be attributed to the fact that melting decreases the thickness along  
 779 the longitudinal interior of the ice shelf, which makes secondary grounding harder to  
 780 instigate.

781 The examples given above indicate general features of how a grounding-line retreat is  
 782 triggered on a retrograde slope upstream of a topographic maximum. As noted above,  
 783 other configurations involving more specialised features could be determined by apply-  
 784 ing the analytical machinery developed here on a case by case basis. This includes the  
 785 prescription of alternative calving laws, nonlinear bed topographies and a large-scale non-  
 786 linear distributed accumulation field, for example, which are readily accounted for within  
 787 the analytical framework presented here. A suite of additional examples is provided in  
 788 the supplementary document demonstrating the construction of the bifurcation diagrams  
 789 for nonlinear bed topographies, as well as a case of large-scale distributed accumulation  
 790 field. The approach of constructing the stability diagram provides both conceptual in-  
 791 sight into conditions for tipped retreat to trigger and considerable numerical efficiency



792 for scenario exploration and sensitivity analysis, and could provide a useful complement  
793 to numerical simulation.

## 794 **7. Conclusions**

795 In this paper, I have analysed the mechanisms underlying the onset of and suppression  
796 of marine ice sheet instability. A central conclusion is that the onset of instability has the  
797 characteristic of a ‘cliff edge’ with an abrupt transition from a mode of easily reversible  
798 ‘stable’ retreat into a mode of almost irreversible ‘tipped retreat’. The tipping points  
799 are identified as occurring abruptly below thresholds of parametric variation and occur  
800 at the vanishing of steady-state branches. The grounding-line positions at which these  
801 parametric thresholds are crossed can occur either midway along a retrograde slope  
802 or at a topographic maximum. A complete regime diagram moving continuously away  
803 from the unbuttressed case was constructed and provides a clear visual demonstration of  
804 how buttressed tipping points are distinct from unbuttressed tipping points. The regime  
805 diagram illustrates that for certain modes of tipping, the long-term trajectory of the ice  
806 sheet’s evolution is dependent on hysteresis (for example whether it has already tipped  
807 into instability), as applies to an unbuttressed tipping transition. For others, the long-  
808 term recovery or collapse of the ice sheet does not depend on hysteresis. That is, certain  
809 parameter values are guaranteed unconditionally to result in stabilisation or collapse  
810 without reference to the initial state of the system (for example, whether the grounding  
811 line has already tipped). This situation is found to apply if tipping is induced by a loss  
812 of ice-shelf buttressing, for which there is an abrupt switch between guaranteed stability  
813 (or recovery from a previously tipped state) and guaranteed retreat across the tipping  
814 threshold. For situations where the suppression of marine ice sheet instability is controlled  
815 by the buttressing force, the basal condition of the ice sheet plays almost no role in setting  
816 the conditions for triggering instability, differing significantly from unbuttressed tipping.  
817 The critical conditions for buttressing-controlled tipping depend primarily on the details  
818 of the ice-shelf dynamics, with control of tipping being related to the length, lateral drag  
819 parameters, calving position, and melt rate of the ice shelf.

820 A method of constructing bifurcation diagrams for grounding lines was developed in  
821 which steady states, the direction in which a perturbation from them will migrate, and  
822 the prediction of secondary grounding of the ice shelf, are each integrated systematically.  
823 The direction of grounding-line migration inferred from the stability diagram was con-  
824 firmed using time-dependent solutions of the governing quasi-two-dimensional equations.  
825 A remarkable feature is that the critical prediction of secondary grounding in steady  
826 state simply overrides the direction of grounding-line migration derived under an assump-  
827 tion that the buttressing force stems from lateral stresses alone, to imply unconditional  
828 advancement. There is therefore a sharp transition in the direction of grounding-line  
829 migration across a parametric tipping point.

830 For ocean depths sufficiently low that the topography allows for an unstable grounding-  
831 line position in the unbuttressed case, the effect of lateral stresses on a positive bed slope  
832 is to cause the unstable steady state to move upstream. For these situations, the hysteresis  
833 effect noted previously for the unbuttressed case is possible, but becomes harder to pro-  
834 duce. At a critical value, the unstable steady state is abruptly invalidated by secondary  
835 grounding, with the steady-state ice-shelf profile necessary to sustain the steady state  
836 predicted to penetrate the bedrock. Remarkably, the prediction of positive-feedback re-  
837 treat without secondary grounding is simply overridden by a prediction of unconditional  
838 advance. The prediction of secondary grounding in steady state is confirmed to lead to  
839 unconditional advance of the grounding line even if the grounding line is initiated far up-

840 stream into territory where it would undergo potentially rapid positive-feedback tipped  
841 retreat if the geometry were such as to preclude secondary grounding. By forming brief,  
842 glancing contacts with the bedrock in the vicinity of the grounding line, the ice shelf  
843 generates an additional time-averaged buttressing force that far exceeds that developed  
844 by lateral drag directly and is sufficiently powerful to suppress grounding-line retreat  
845 almost unconditionally. The possibility for hysteresis is thus sharply eliminated if the  
846 criterion for secondary grounding is satisfied.

847 The glancing contacts that can arise during the recovery of a retreated grounding  
848 line develop a tertiary mechanical component – intermediate to the fully grounded and  
849 floating regions – referred to as the ‘marginal-flotation regime’. This regime replaces the  
850 notion of a grounding line with a grounding *area*. Along this region, the thickness of  
851 the ice sheet straddles the critical thickness for flotation, with the base of the ice shelf  
852 ‘hovering’ above the bedrock with intermittent contact. The creation of this zone is caused  
853 by the thickening of the interior of the ice shelf by lateral stresses, which induces the  
854 contact, combined with a switchback mechanism in the governing conditional momentum  
855 equation creating rapid oscillations between its floating and grounded components. The  
856 existence of the marginal flotation zone may be a hallmark of a marine ice sheet that  
857 is regenerating from a former inducement of tipped retreat, and may be an important  
858 mechanism for generating marine ice sheets during periods of glaciation.

859 For the case where the ocean depth is sufficiently deep that there is no steady steady in  
860 the unbuttressed case, unconditional retreat of the grounding line occurs for all values of  
861 the coefficient of lateral drag below a critical tipping-point value. Above the threshold,  
862 lateral stresses produce a new branch of stable steady states. It was found that even  
863 marginally above the threshold, the ice sheet is completely secure against permanent  
864 tipping, even following a total collapse of the ice shelf. However, if the parameters in  
865 the system vary such as to produce a change to subcritical values, destabilisation of  
866 the ice sheet occurs. A natural mode of destabilisation was demonstrated in which the  
867 grounding line retreats ‘stably’ along the stable branch in a quasi-steady manner before  
868 transitioning to ‘tipped’ retreat once the steady-state branch vanishes and the tipping  
869 point for buttressed stability is passed (at least with the assumption that the ice shelf  
870 can regrow to its former calving position). Following the transition to tipped retreat, the  
871 system will always fail to recover following a parametric restoration to former values.

872 However, the recovery of a tipped grounding line was determined to be possible fol-  
873 lowing a recovery of parameters to values slightly more secure than the values that were  
874 necessary to trigger tipping in the first place. The restoration of the grounding line al-  
875 ways occurs as a consequence of the ice shelf making secondary contact with the bedrock,  
876 forming an ice rise or marginal-flotation zone. Lateral stresses allow this mode of recovery  
877 to become more feasible owing to its development of a considerably thicker ice shelf. The  
878 conditions for regrounding can be almost coincident with the condition for establishing  
879 the steady state from which tipping is critically lost. This result is attributed to the prop-  
880 erty that the grounding-line position necessary to produce regrounding and the position  
881 for a buttressed steady state to form can occur very close together (Pegler 2018). The  
882 bifurcation diagrams show that the conditions for secondary contact are easier to attain  
883 than those necessary to instigate reversal of a tipped grounding line in the absence of any  
884 secondary grounding. The reversal of tipped grounding-line retreat is therefore dependent  
885 on and/or occurs with the formation of an ice rise or marginal flotation zone.

886 A complete regime diagram for tipping and recovery of a grounding line was con-  
887 structed, showing that there are two distinct criteria that can trigger a critical transition  
888 to runaway grounding-line retreat upstream of a topographic maximum. One is the but-  
889 tressed threshold described above. The other is the unbuttressed threshold. The failure

of both of these distinct criteria was shown to be necessary in order to induce tipping of the ice sheet on a retrograde slope.

Transitions to tipped retreat induced by the retreat of a calving front or the increase in the rate of basal melting of the ice shelf were demonstrated. In the latter case, the steady-state grounding-line position was found to be relatively insensitive to melt rate before an abrupt transition to tipped retreat occurs above a critical melt rate. The tipping point resulting from an increase in melt rate produces an abrupt transition from very gradual stable retreat to sudden tipped retreat. The conditions necessary to reverse the tipped retreat driven by an increase in melting was found to be relatively harder to attain as compared to tipping induced by calving or lateral softening.

The results of this work provide a foundation for understanding the processes leading to a regional or large-scale collapse of the WAIS and paleo ice sheets. An overarching conclusion is that lateral stresses exerted on ice shelves introduces a remarkably important effect for maintaining global stability. The sustainment of mass in a marine ice sheet depends on two different controls: the setting of the grounding line, and the setting of the interior thickness upstream of the grounding line. Importantly, these properties are controlled by different physical processes and parameters. Either one of these must be the weak link in maintaining a ‘healthy’ marine ice sheet. In regards to the future of the WAIS, it can be anticipated that the control of the grounding line is likely to provide the weaker of the two links. The importance of ice shelves can be attributed to their independent contribution to the strengthening of this weakest link. The stability of the WAIS is therefore likely to be contingent on the physical processes controlling the sustainment of ice shelves and their lateral contact.

I am grateful to Grae Worster for comments on an early draft of this paper. I would like to thank the three anonymous referees whose comments led to significant improvement of the paper. I also thank Hilmar Gudmundsson, Ian Hewitt, and Brent Minchew for helpful discussions.

#### REFERENCES

- BAMBER, J. L., RIVA, R. E. M., VERMEERSEN, B. L. A. & LEBROCQ, A. M. 2009 Reassessment of the potential sea-level rise from a collapse of the West Antarctic Ice Sheet. *Science* **324** (5929), 901–903.
- CHUGUNOV, V. A. & WILCHINSKY, A. V. 1996 Modelling of marine glacier and ice-sheet–ice-shelf transition zone based on asymptotic analysis. *Ann. Glac.* **23**, 59–67.
- CUFFEY, K. M. & PATERSON, W. S. B. 2010 *The physics of glaciers*, 4th edn. Academic Press.
- DUPONT, T. K. & ALLEY, R. B. 2005 Assessment of the importance of ice-shelf buttressing to ice-sheet flow. *Geophys. Res. Lett.* **32**, F03009.
- FAVIER, L., DURAND, G., CORNFORD, S. L., GUDMUNDSSON, G. H., GAGLIARDINI, O., GILLET-CHAULET, F. & BROCCO, M. LE 2014 Retreat of Pine Island Glacier controlled by marine ice-sheet instability. *Nature Climate Change* **5** (2), 117–121.
- FOWLER, A. C. 2011 *Mathematical geoscience*. Springer.
- GAGLIARDINI, O., DURAND, G., ZWINGER, T., HINDMARSH, R. C. A. & MEUR, E. LE 2010 Coupling of ice-shelf melting and buttressing is a key process in ice-sheets dynamics. *Geo. Res. Lett.* **37**, L14501.
- GOLDBERG, D., HOLLAND, D. M. & SCHOOF, C. 2009 Grounding line movement and ice shelf buttressing in marine ice sheets. *J. Geophys. Res.* **114**, F0402.
- GUDMUNDSSON, G. H. 2013 Ice-shelf buttressing and the stability of marine ice sheets. *The Cryosphere* **7**, 647–655.
- GUDMUNDSSON, G. H., KRUG, J., DURAND, G., FAVIER, L. & GAGLIARDINI, O. 2012 The stability of grounding lines on retrograde slopes. *The Cryosphere* **6**, 1497–1505.
- HANNA, E. *et al.* 2013 Ice-sheet mass balance and climate change. *Nature* **498**, 51–59.

- 939 HINDMARSH, R. C. A. 2012 An observationally validated theory of viscous flow dynamics at  
940 the ice-shelf calving front. *J. Glaciol.* **58**, 375–387.
- 941 HUGHES, T. J. 1981 The weak underbelly of the West Antarctic ice sheet. *J. Glaciol.* **27** (97),  
942 518–25.
- 943 KOWAL, K. N., PEGLER, S. S. & WORSTER, M. G. 2016 Dynamics of laterally confined marine  
944 ice sheets. *J. Fluid Mech.* **790**, R2.
- 945 MACAYEAL, D. R. 1989 Large-scale ice flow over a viscous basal sediment: Theory and appli-  
946 cation to Ice Stream B, Antarctica. *J. Geophys. Res.* **94**, 4071–4087.
- 947 MUSZYNSKI, I. & BIRCHFIELD, G. E. 1987 A coupled marine ice-stream–ice-shelf model. *J.*  
948 *Glaciol.* **33**, 3–15.
- 949 NICK, F. M., VAN DER VEEN, C. J., VIELI, A. & BENN, D. I. 2010 A physically based calving  
950 model applied to marine outlet glaciers and implications for the glacier dynamics. *J. Glaciol.*  
951 **56** (199), 781–794.
- 952 PEGLER, S. S. 2016 The dynamics of confined extensional flows. *J. Fluid Mech.* **804**, 24–57.
- 953 PEGLER, S. S. 2018 Marine ice sheet dynamics: the impacts of ice-shelf buttressing. *J. Fluid*  
954 *Mech.* Under review.
- 955 PEGLER, S. S., KOWAL, K. N., HASENCLEVER, L. Q. & WORSTER, M. G. 2013 Lateral controls  
956 on grounding-line dynamics. *J. Fluid Mech.* **722**, R1.
- 957 ROBISON, R. A. V., HUPPERT, H. E. & WORSTER, M. G. 2010 Dynamics of viscous grounding  
958 lines. *J. Fluid Mech.* **648**, 363–380.
- 959 SCHOOF, C. 2007a Ice sheet grounding line dynamics: Steady states, stability, and hysteresis.  
960 *J. Geophys. Res.* **112**, F03S28.
- 961 SCHOOF, C. 2007b Marine ice sheet dynamics. Part 1: The case of rapid sliding. *J. Fluid Mech.*  
962 **573**, 27–55.
- 963 SCHOOF, C. 2012 Marine ice sheet stability. *J. Fluid Mech.* **698**, 62–72.
- 964 SCHOOF, C., DAVIS, A. D. & POPA, T. V. 2017 Boundary layer models for calving marine  
965 outlet glaciers. *The Cryosphere* **11**, 2283–2303.
- 966 STUIVER, M., DENTON, G.H., HUGHES, T. J. & FASTOOK, J. L. 1981 *History of the marine*  
967 *ice sheet in West Antarctica during the last glaciation: a working hypothesis*, pp. 319–436.  
968 New York: Wiley-Interscience.
- 969 THOMAS, R. H. & BENTLEY, C. R. 1978 A model for Holocene retreat of the West Antarctic  
970 ice sheet. *Quaternary Research* **2**, 150–170.
- 971 TSAI, V. C., STEWART, A. L. & THOMPSON, A. F. 2015 Marine ice-sheet profiles and stability  
972 under Coulomb basal conditions. *J. Glaciol.* **61**, 205–221.
- 973 WALKER, R. T., HOLLAND, D. M., PARIZEK, B. R., ALLEY, R. B., NOWICKI, S. M. J. &  
974 JENKINS, A. 2013 Efficient flowline simulations of ice shelf–ocean interactions: Sensitivity  
975 studies with a fully coupled model. *J. Phys. Oceanogr.* **43**, 2200–2210.
- 976 WEERTMAN, J. 1974 Stability of the junction of an ice sheet and an ice shelf. *J. Glaciol.* **31**,  
977 3–11.
- 978 WILCHINSKY, A. V. 2009 Linear stability analysis of an ice sheet interacting with the ocean. *J.*  
979 *Glaciol.* **55**, 13–20.
- 980 WILCHINSKY, A. V. & CHUGUNOV, V. A. 2000 Ice stream–ice shelf transition: theoretical  
981 analysis of two-dimensional flow. *Ann. Glaciol.* **30**, 153–162.